Electronic Supplementary Information

Monitoring the hydrogen bond net configuration and the dimensionality of aniline and phenyloxamate by adding 1*H*-pyrazole and isoxazole as substituents for molecular self-recognition

Willian X. C. Oliveira,[†] Walace D. do Pim, [‡] Carlos B. Pinheiro,[§] Yves Journaux,[⊥] Miguel Julve[‖] and Cynthia L. M. Pereira*,[†]

[†]Departamento de Química, Instituto de Ciências Exatas, Universidade Federal de Minas Gerais. Av. Pres. Antônio Carlos, 6620, Pampulha, 31270-901 Belo Horizonte, Minas Gerais, Brazil;

[‡]Centro Federal de Educação Tecnológica de Minas Gerais, Av. Amazonas, 5253, Nova Suíça, 30421-169 Belo Horizonte, Minas Gerais, Brazil.

[§]Departamento de Física, Instituto de Ciências Exatas, Universidade Federal de Minas Gerais. Av. Pres. Antônio Carlos, 6620, Pampulha, 31270-901 Belo Horizonte, Minas Gerais, Brasil;

[⊥] Sorbonne Universités UPMC Univ Paris 06, CNRS UMR 8232, Institut Parisien de Chimie Moléculaire, Paris, France

[‖]Instituto de Ciencia Molecular (ICMol), Universitat de València, C/ Catedrático José Beltrán 2, 46980 Paterna, València, Spain.

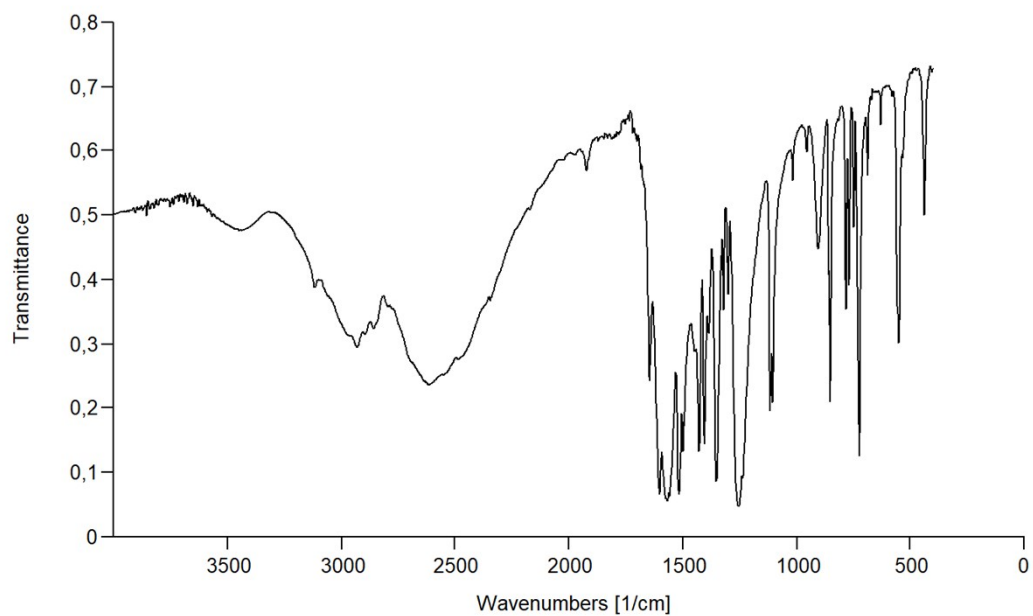*Corresponding author e-mail: cynthialopes@ufmg.br
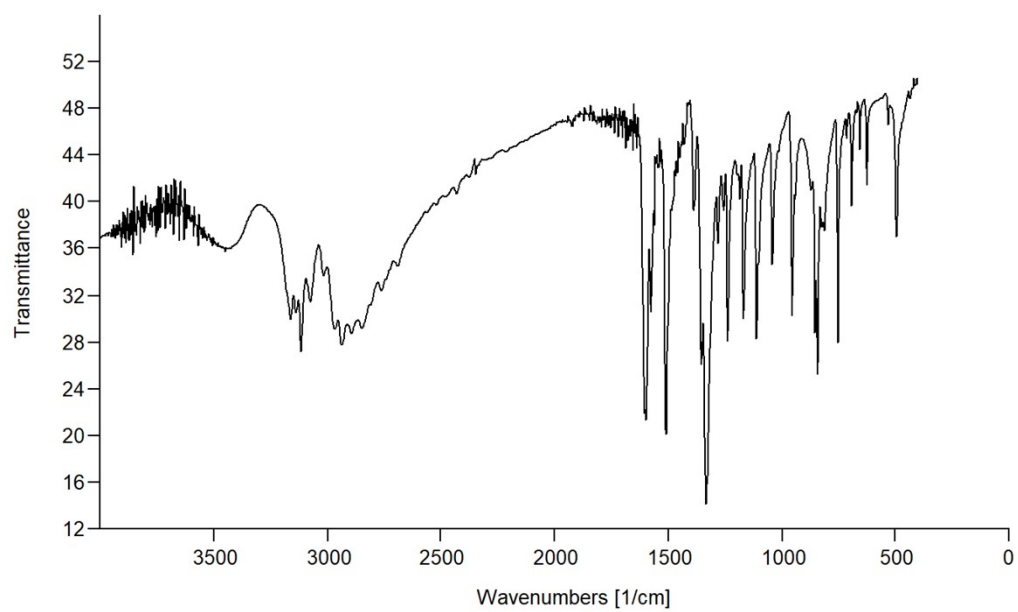
Figure S1 – IR spectrum of **1**.
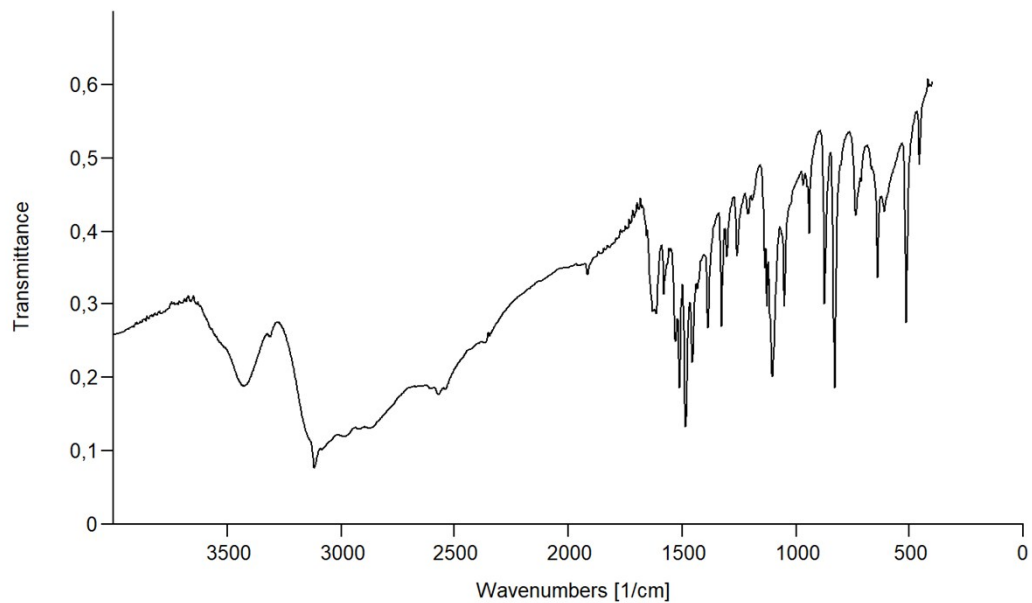

Figure S2 – IR spectrum of **2a**.
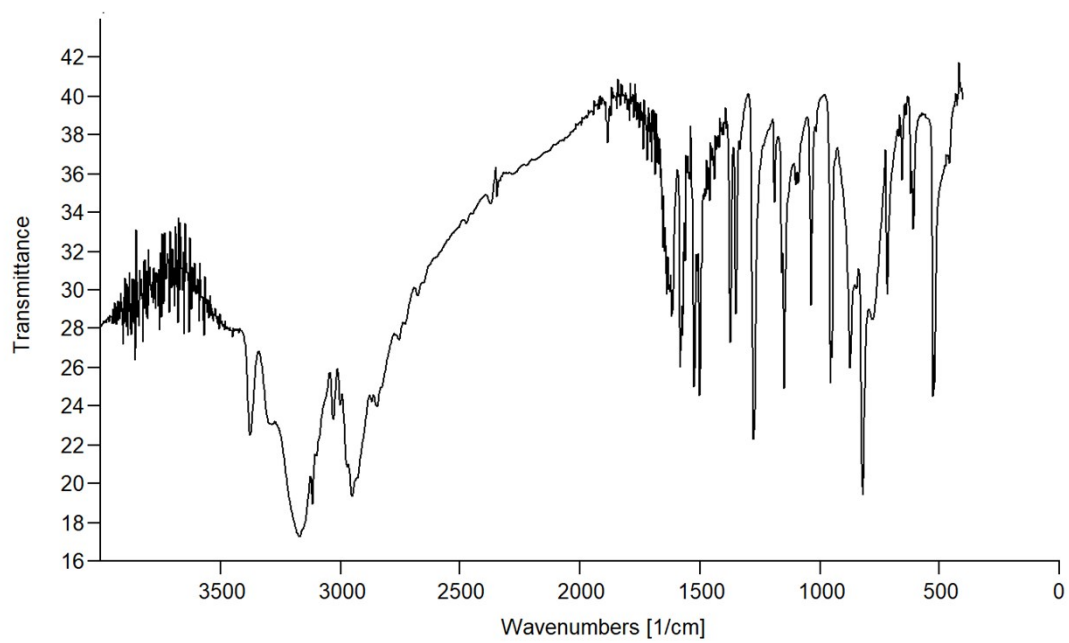
Figure S3 – IR spectrum of **2b**.
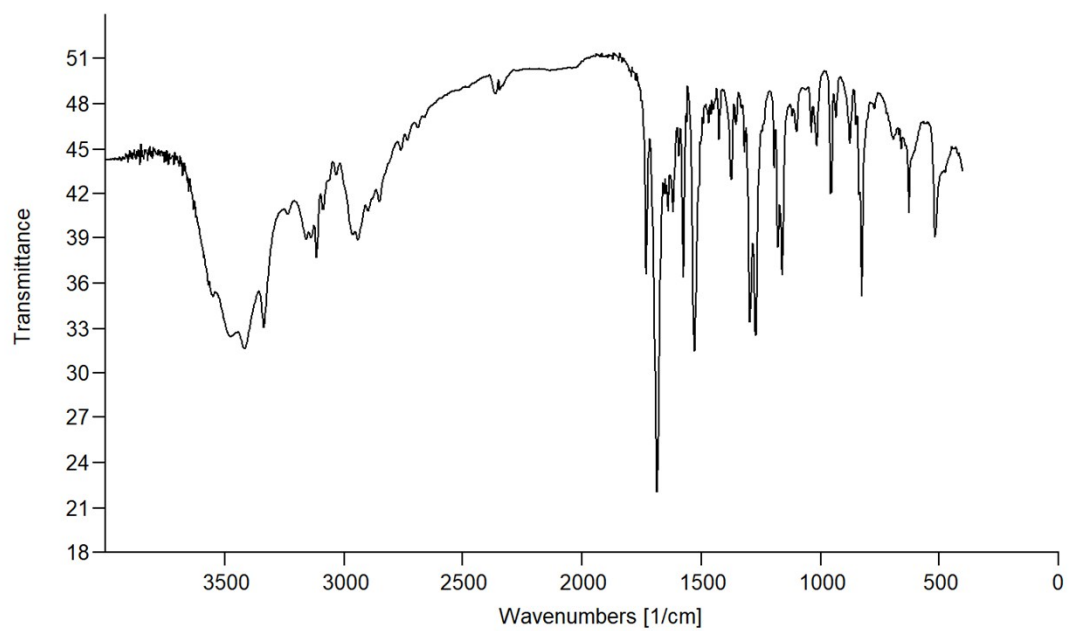

Figure S4 – IR spectrum of **2c**.
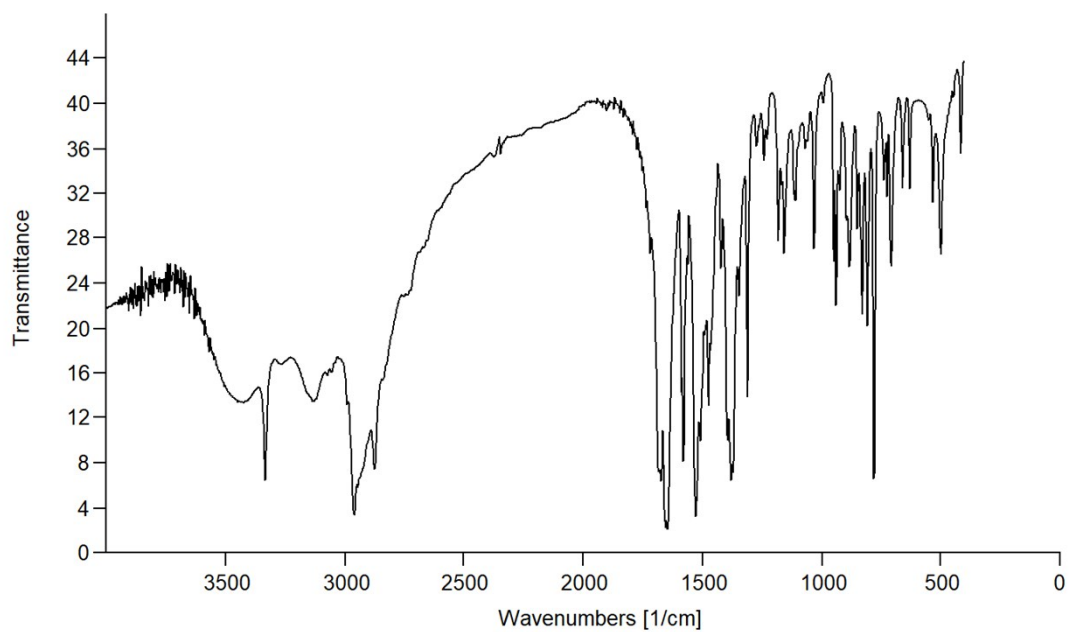
Figure S5 – IR spectrum of **2d**.
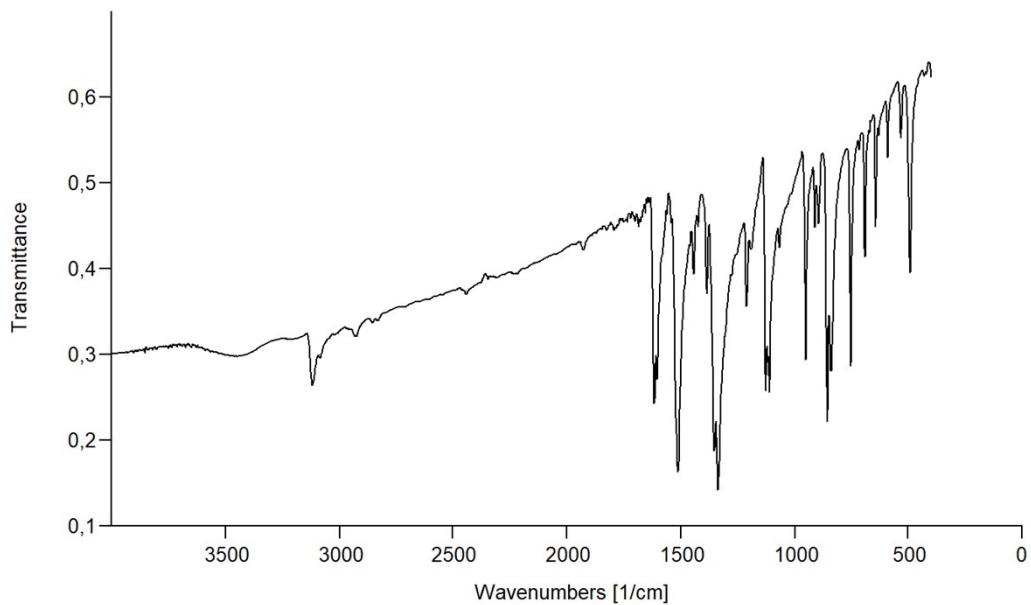

Figure S6 – IR spectrum of **2e**.
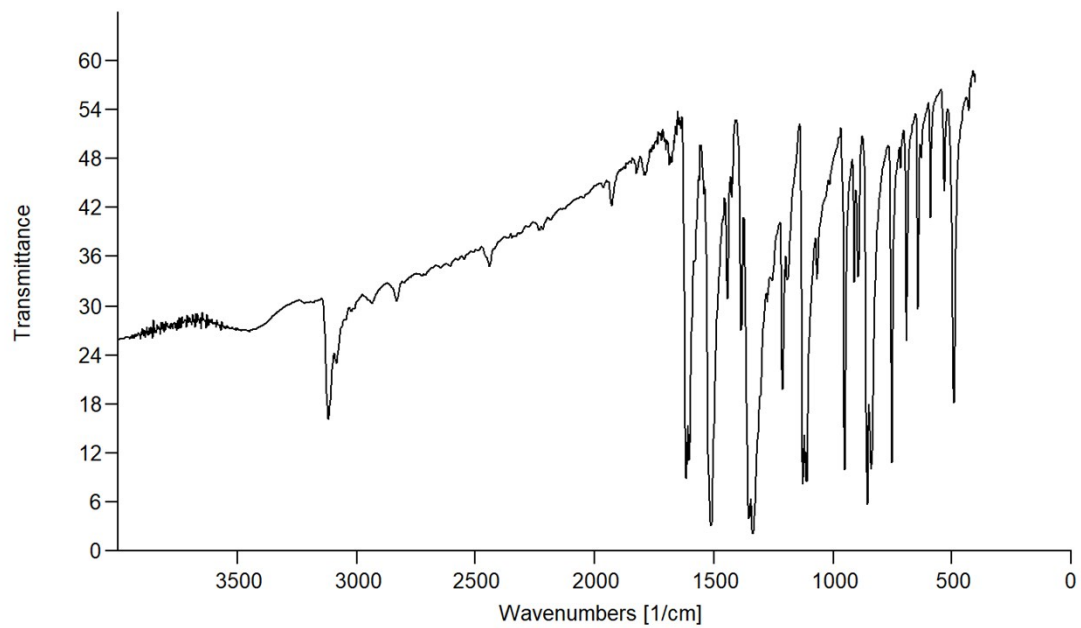
Figure S7 – IR spectrum of **3a**.
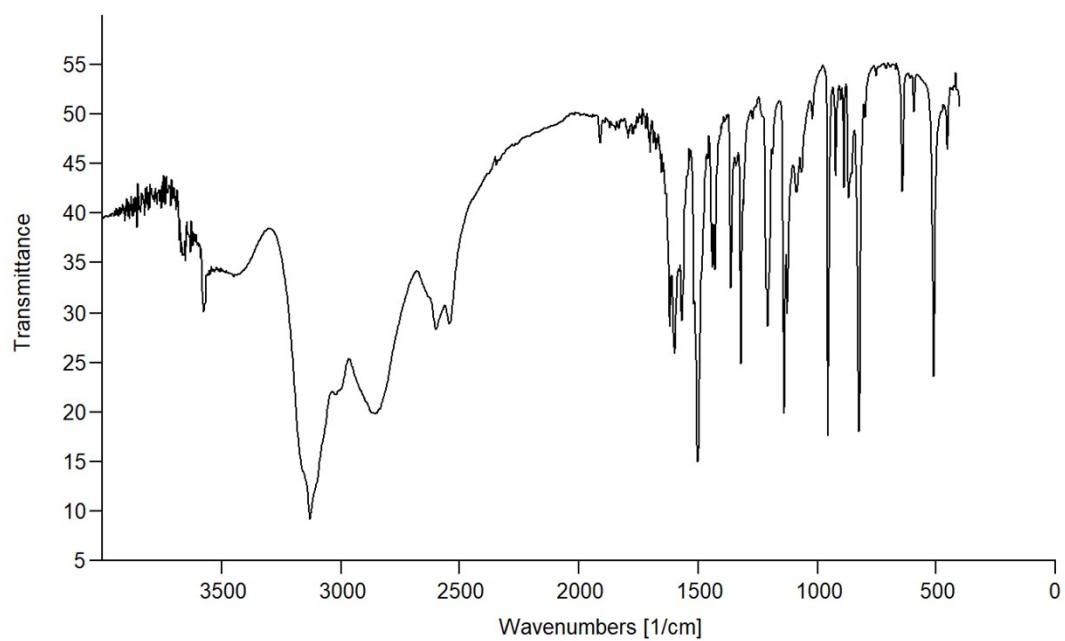

Figure S8 – IR spectrum of **3b**.
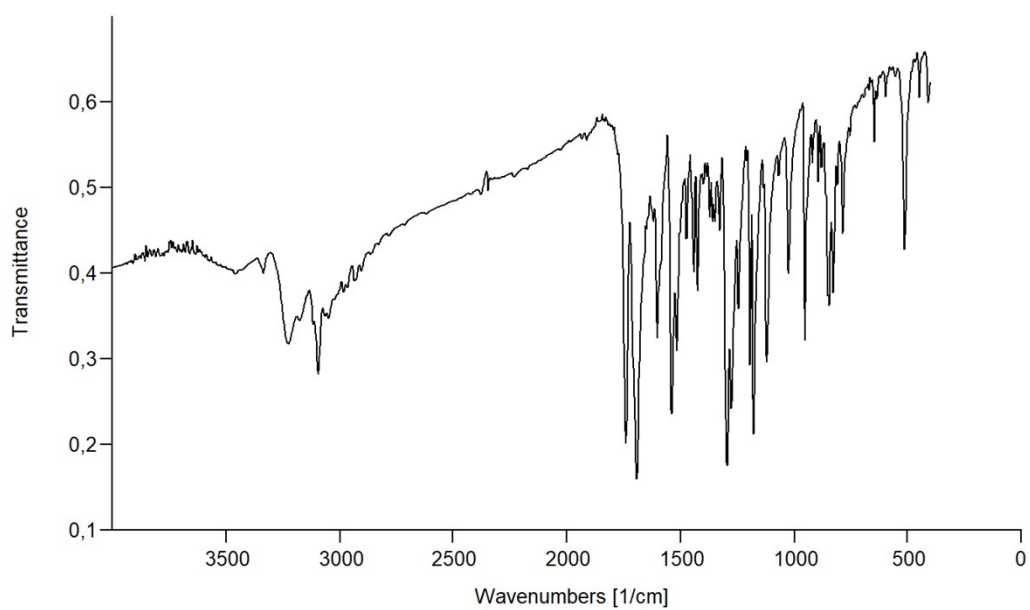
Figure S9 – IR spectrum of **3c**.

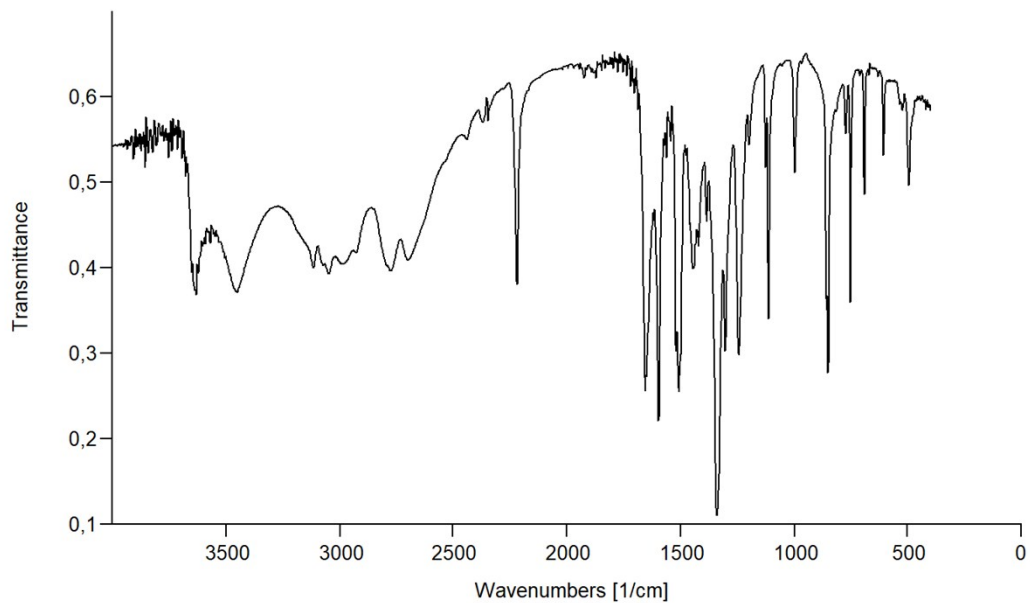**Figure S10** – IR spectrum of **3d**.

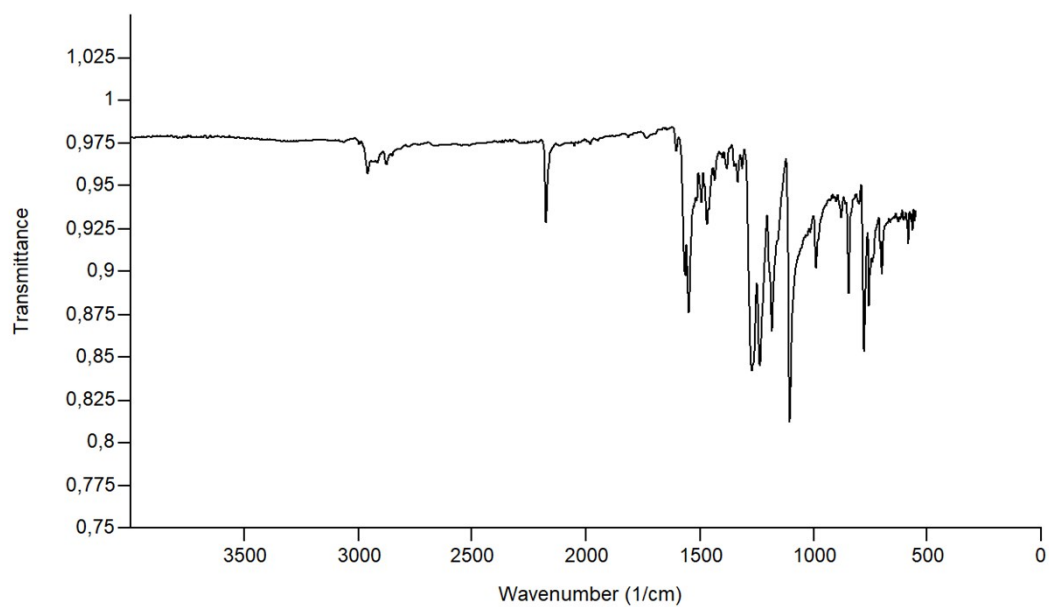**Figure S11** – IR spectrum of **3e**.
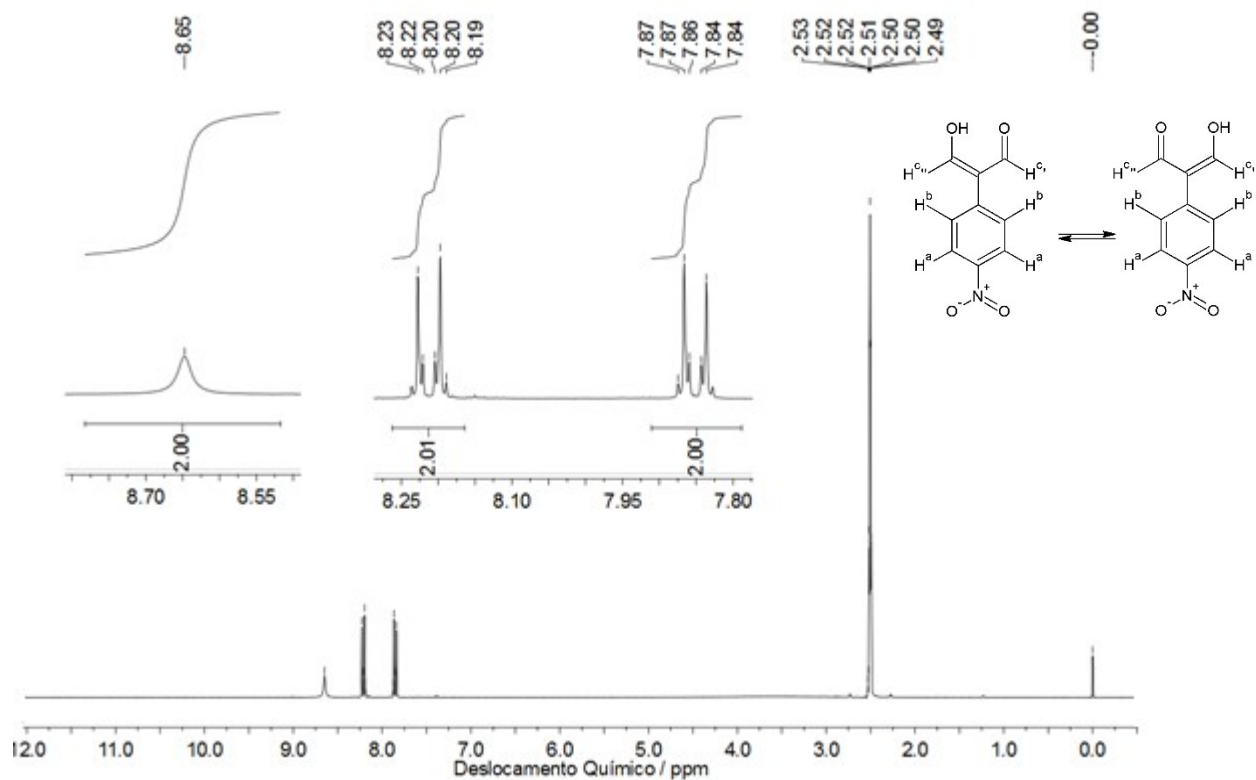

Figure S12 – IR spectrum of **3f**.

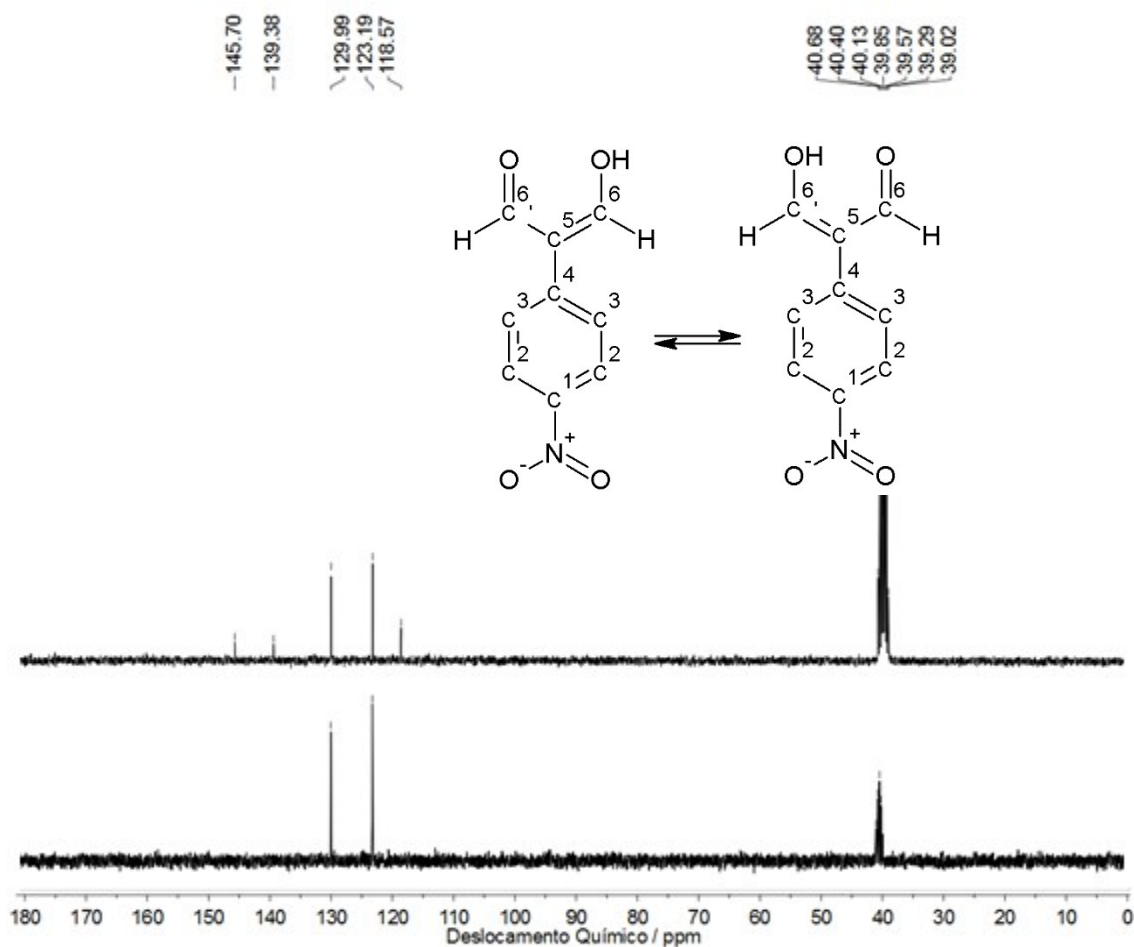**Figure S13** – ^1H NMR spectrum of **1** in dmso-d_6 at 300 MHz.

Figure S14 – ^{13}C NMR, at 75 MHz, (top) and DEPT-135 (bottom) spectra for **1** .

Figure S15 – ^{1}H NMR spectrum of **2a** in dmso-d$_6$ at 200 MHz.

Figure S16 – ^{13}C NMR, at 50 MHz, (top) and DEPT-135 (bottom) spectra for **2a**.

Figure S17 – ^{1}H NMR spectrum of **2b** in dmso-d$_6$ at 200 MHz.

Figure S18 – ^{13}C NMR, at 50 MHz, (top) and DEPT-135 (bottom) spectra for **2b** .

Figure S19 – ^{1}H NMR spectrum of **2c** in dmso-d_6 at 300 MHz.

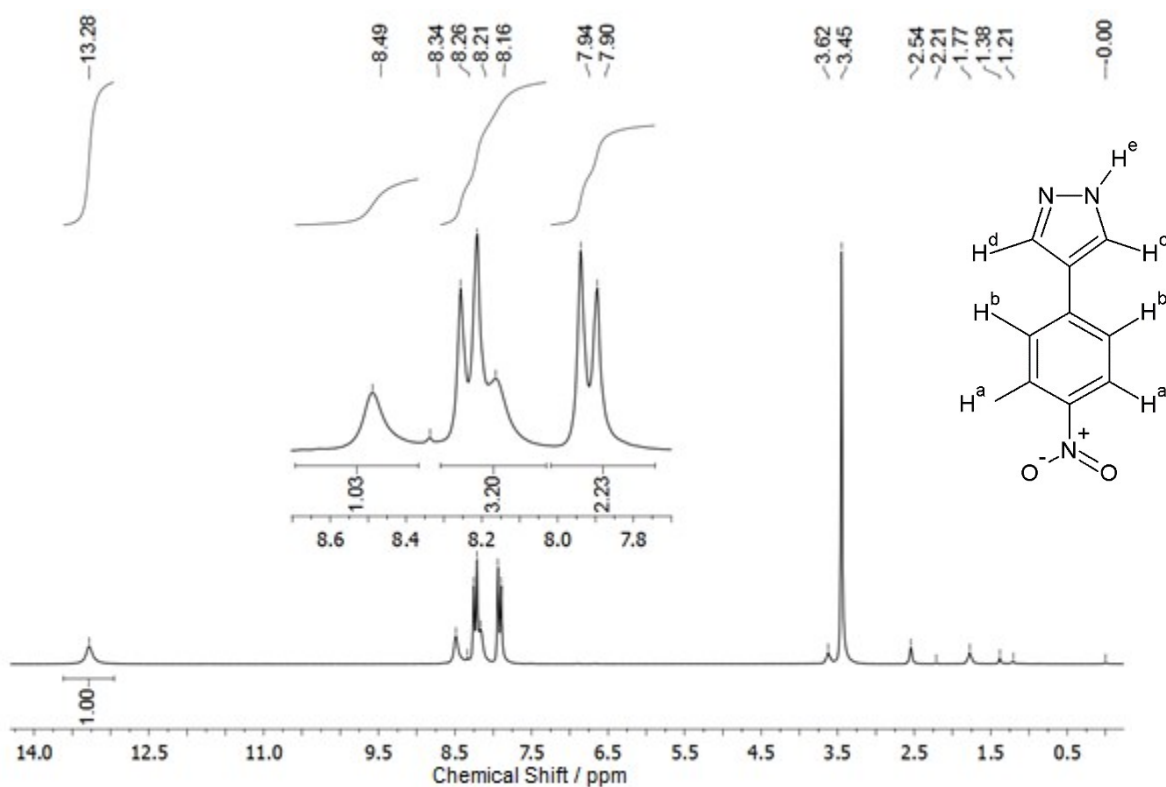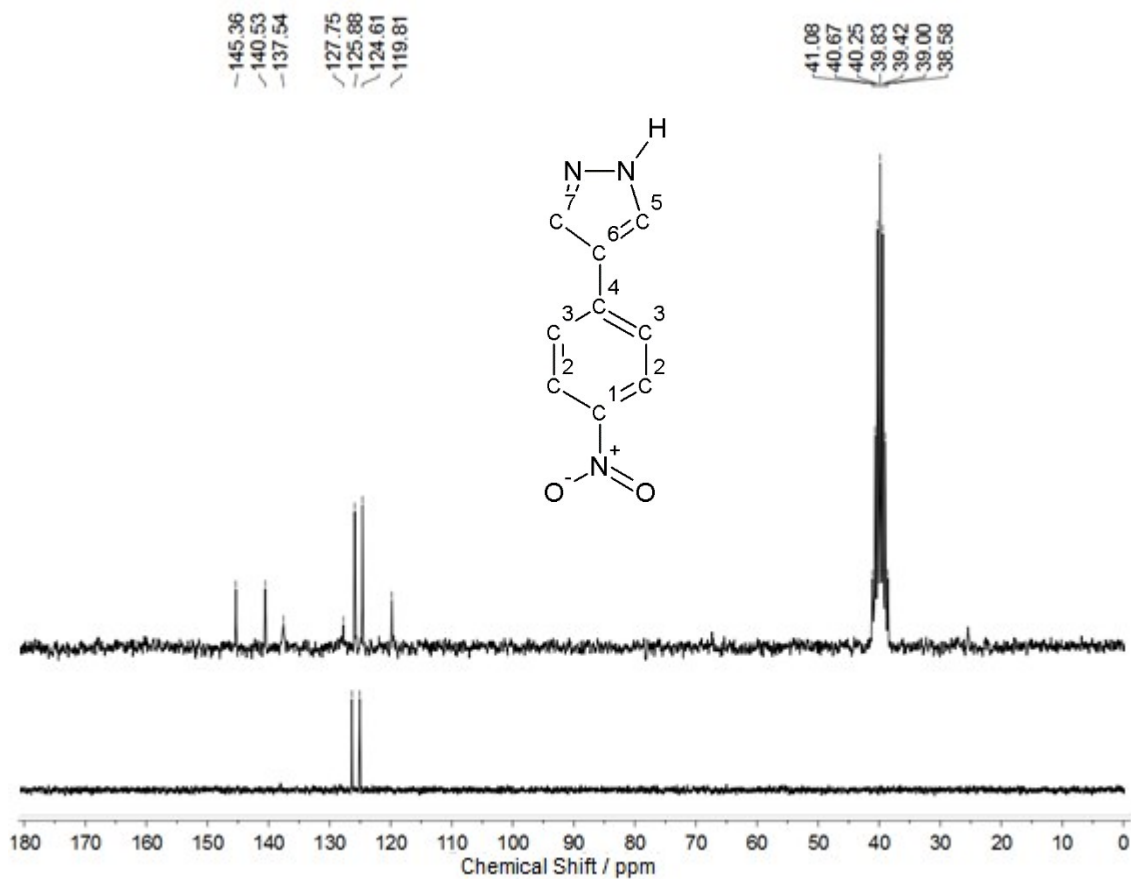**Figure S20** – ^{13}C NMR, at 75 MHz (top) and DEPT-135 (bottom) spectra for **2c**.

Figure S21 – ^1H NMR spectrum of **2d** in dmso-d_6 at 300 MHz.

Figure S22 – ^{13}C NMR, at 75 MHz (top) and DEPT-135 (bottom) spectra for **2d** .
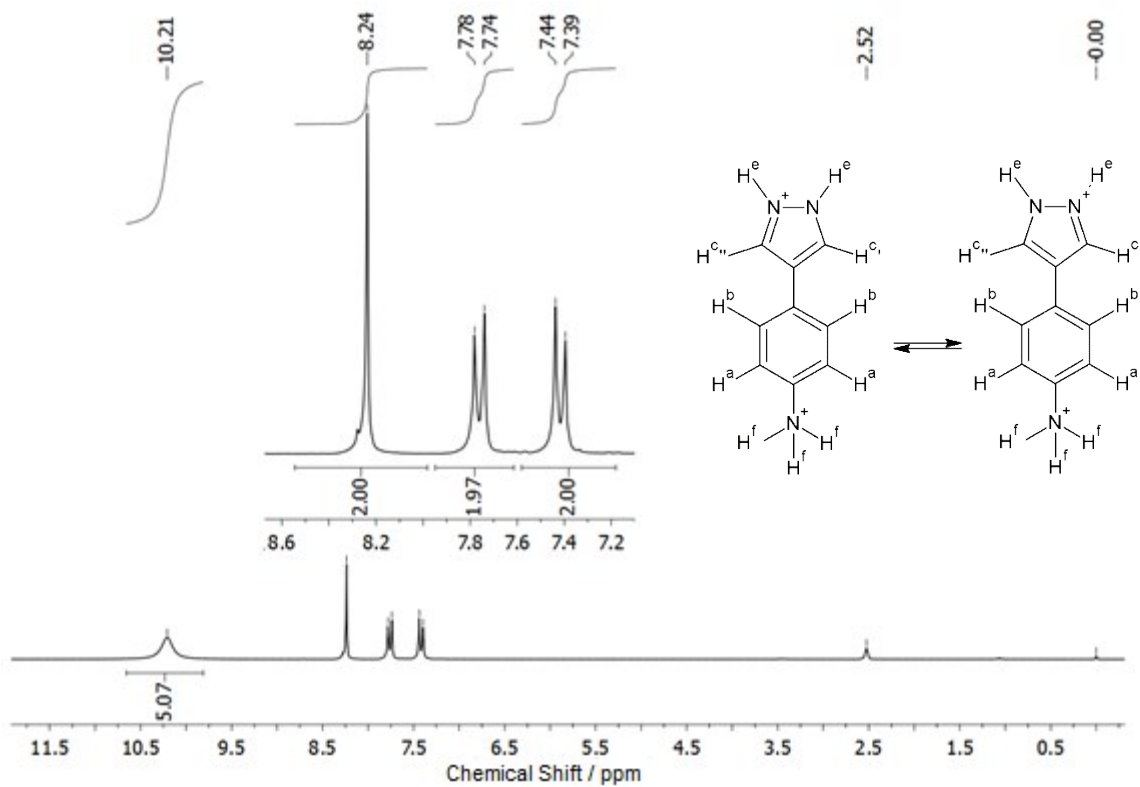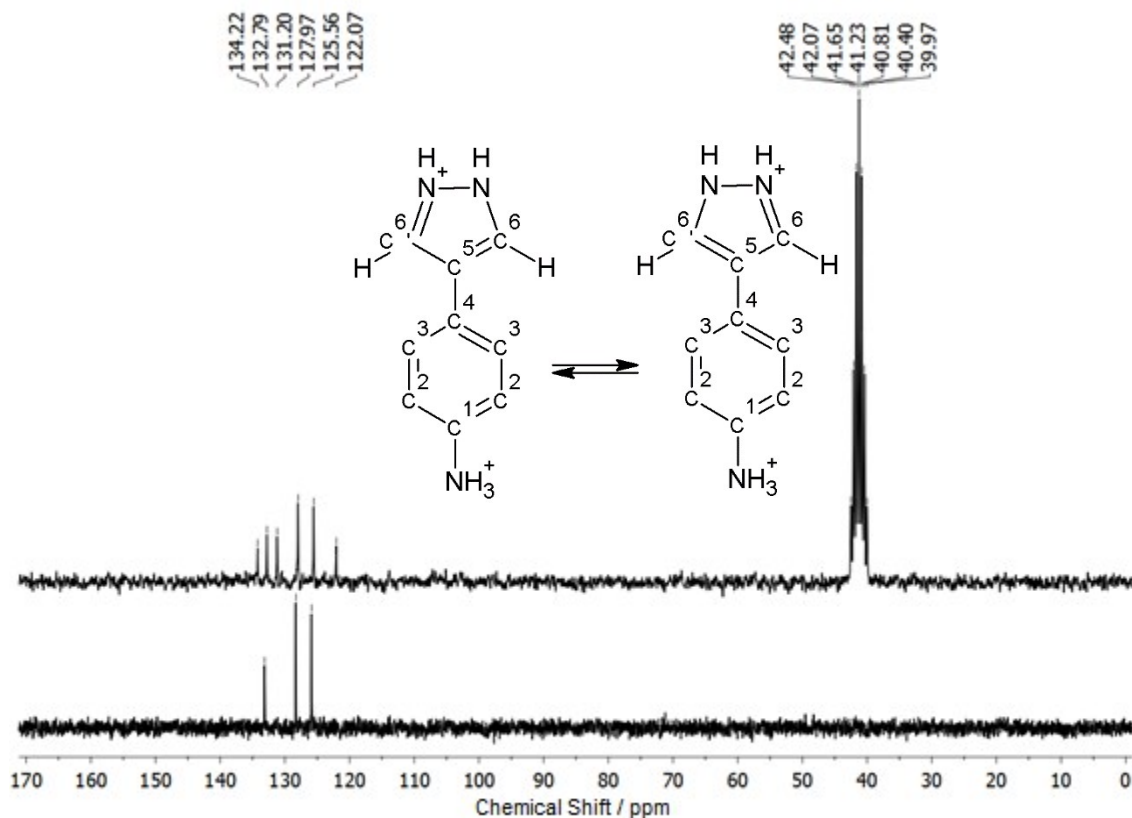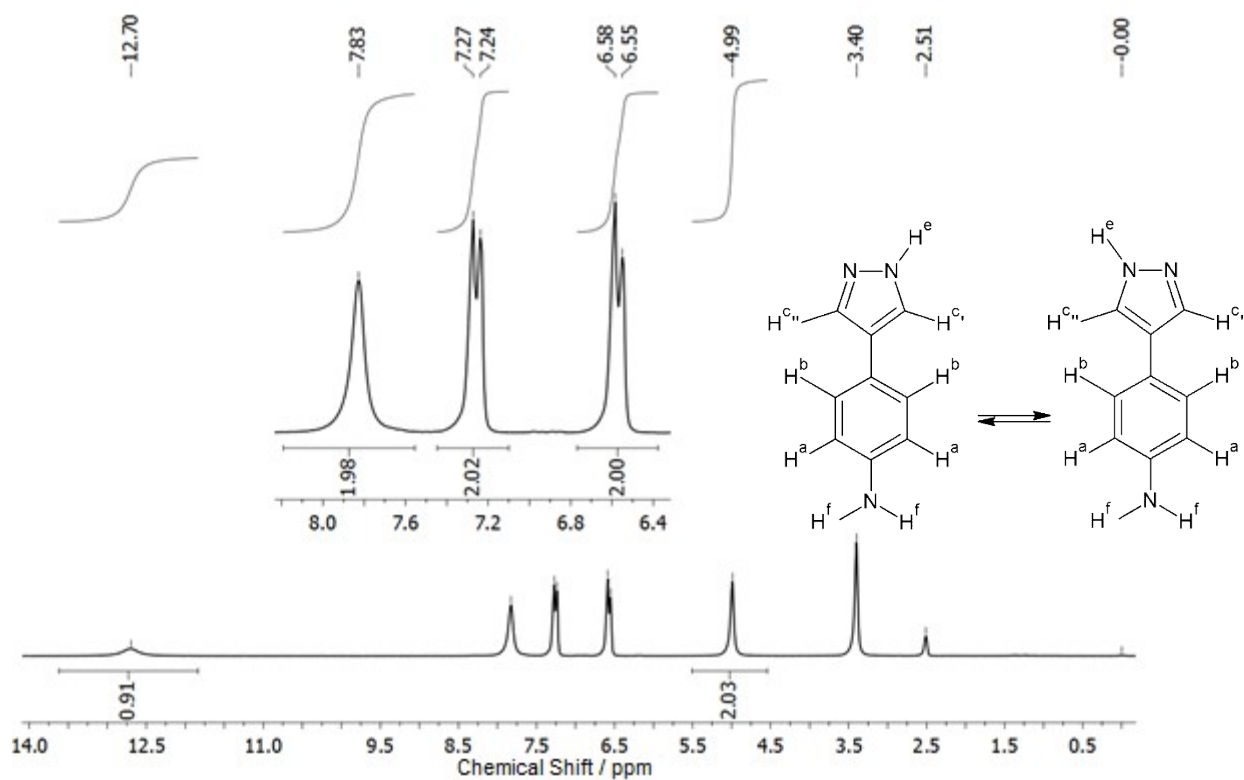
Figure S23 – ^{1}H NMR spectrum of **2e** in dmso-d$_6$ at 300 MHz.
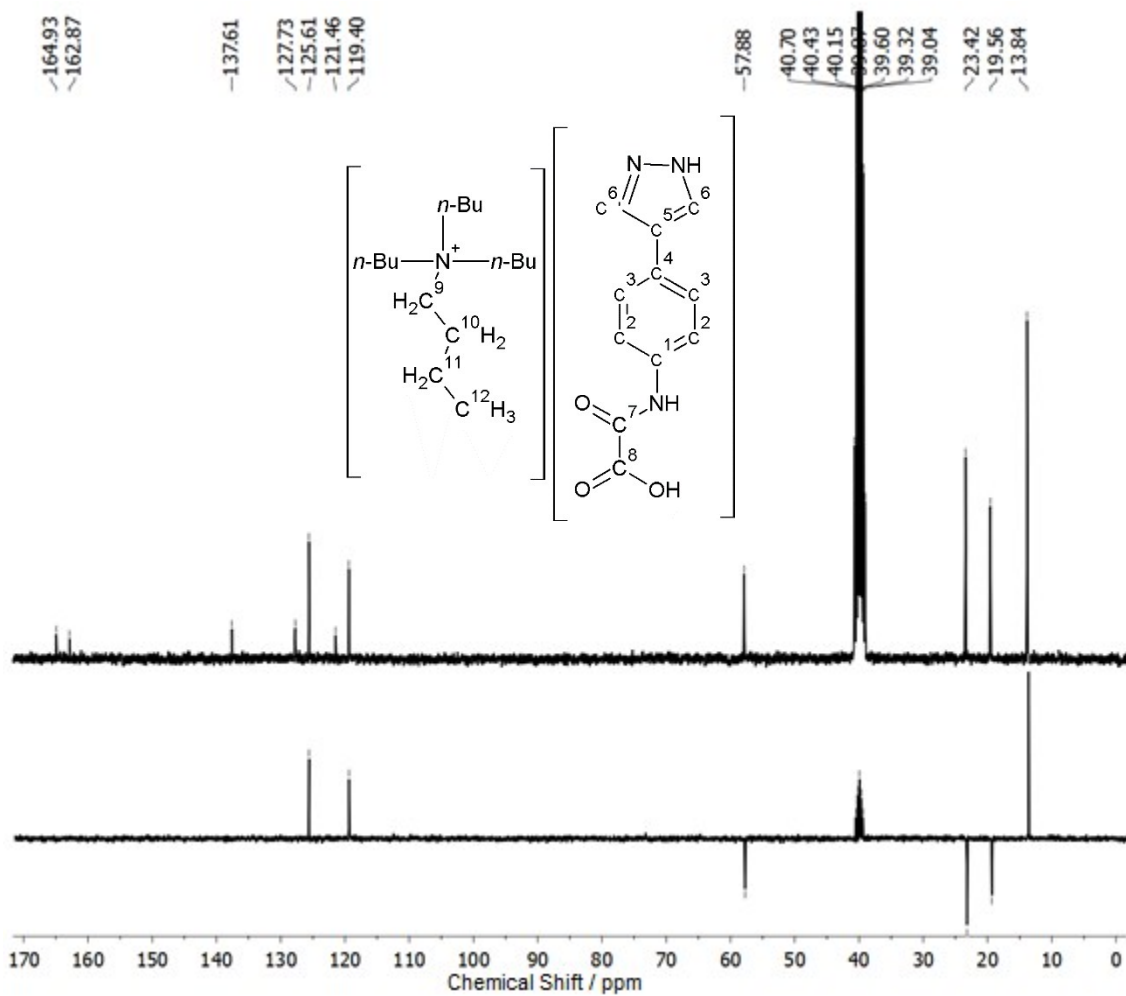
Figure S24 – ^{13}C NMR, at 75 MHz (top) and DEPT-135 (bottom) spectra for **2d**.

Figure S25 – ^{1}H NMR spectrum of **3a** in dmso-d_6 at 200 MHz.

Figure S26 – ^{13}C NMR, at 50 MHz, (top) and DEPT-135 (bottom) spectra for **3a**.

Figure S27 – ^{1}H NMR spectrum of **3b** in dmso-d$_6$ at 300 MHz.
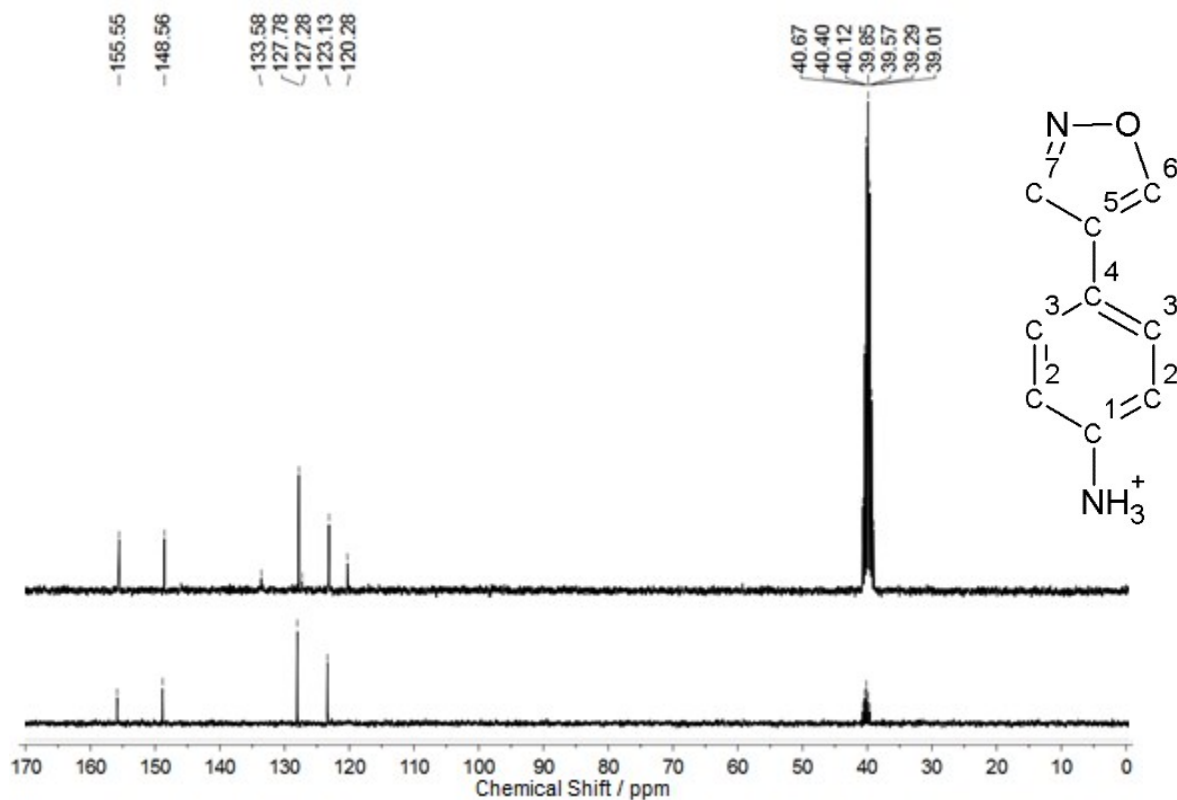
Figure S28 – ^{13}C NMR, at 75 MHz, (top) and DEPT-135 (bottom) spectra for **3b**.

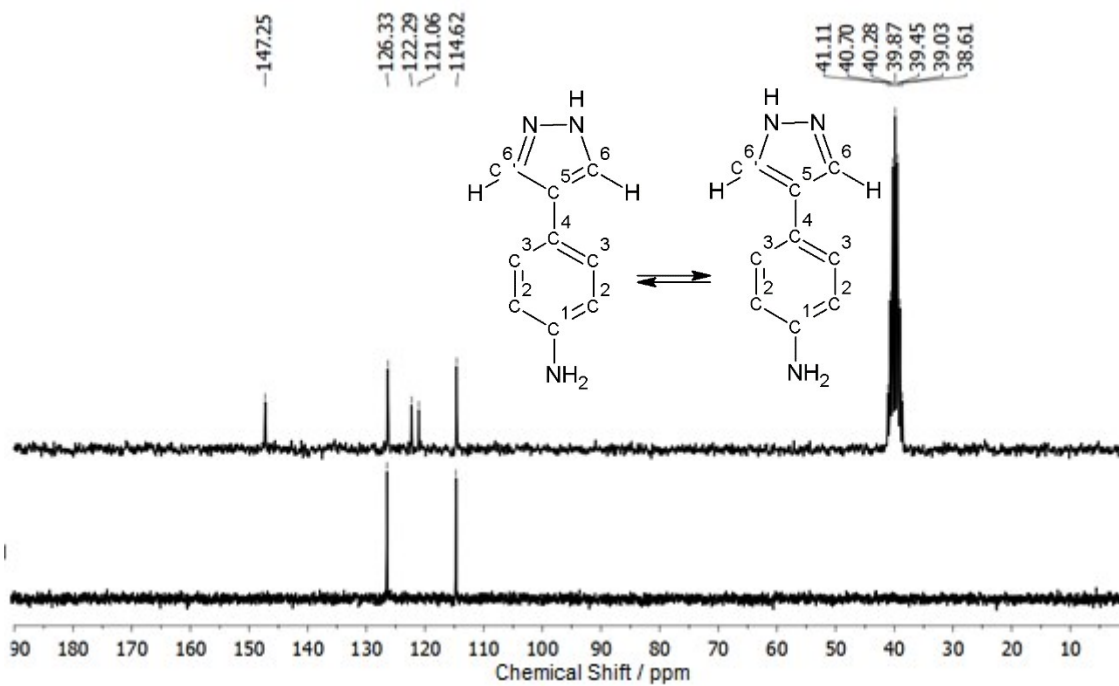**Figure S29** – ^{1}H NMR spectrum of **3c** in dmso-d$_6$ at 300 MHz.

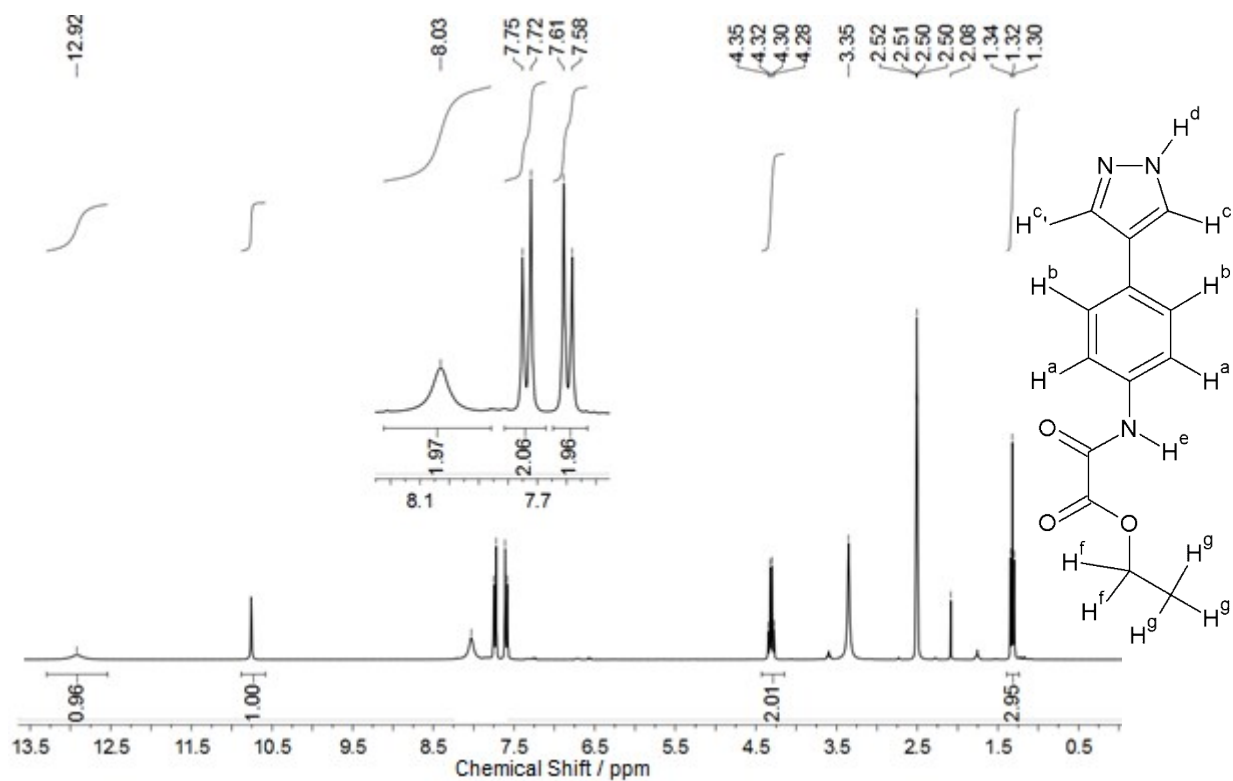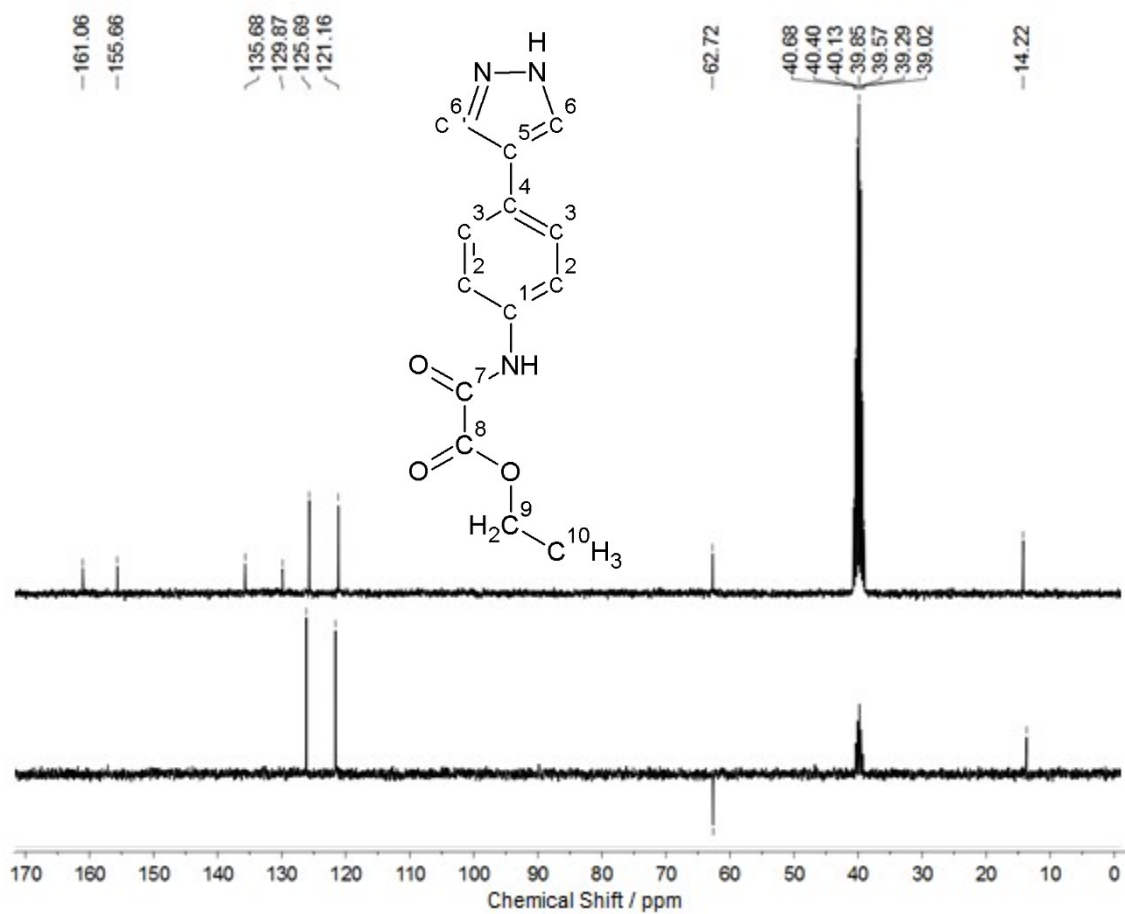**Figure S30** – ^{13}C NMR, at 75 MHz, (top) and DEPT-135 (bottom) spectra for **3c**.
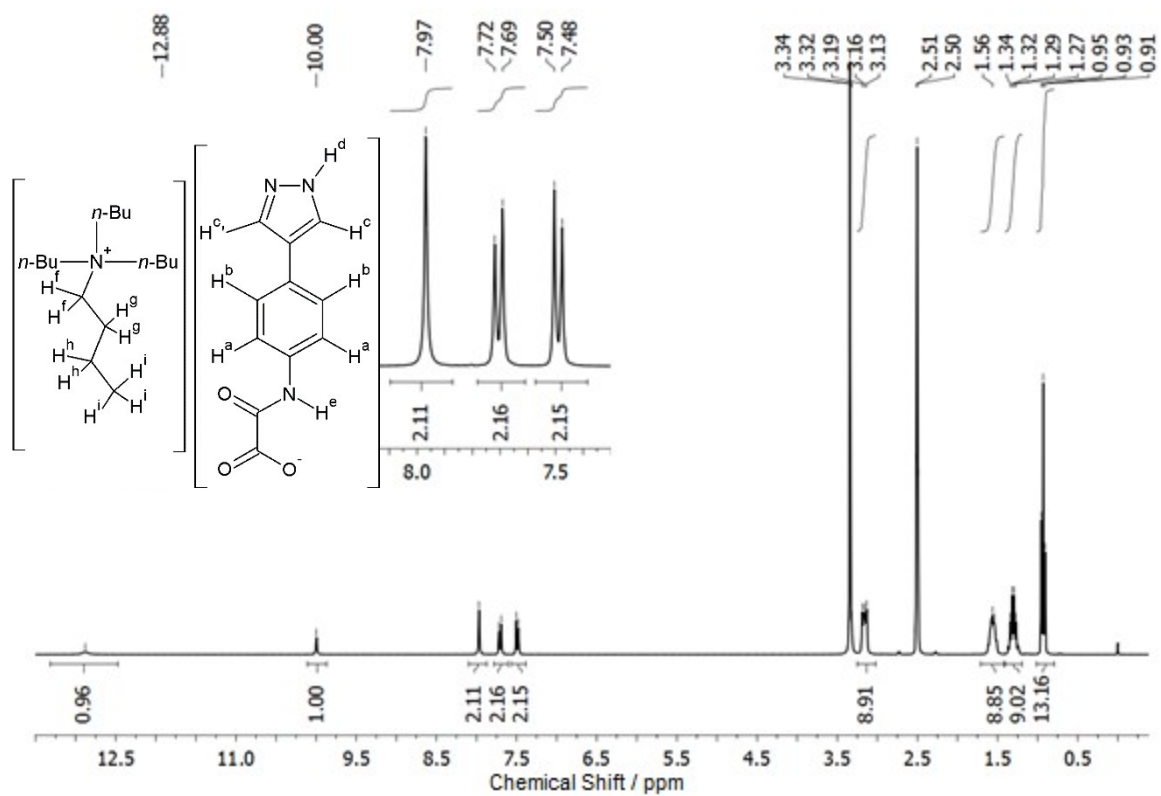

Figure S31 – ^{1}H NMR spectrum of **3d** in dmso-d_6 at 300 MHz.

Figure S32 – ^{13}C NMR, at 75 MHz, (top) and DEPT-135 (bottom) spectra for **3d**.

**Figure S33** – ^{1}H NMR spectrum of **3e** in CD$_3$CN at 400 MHz.
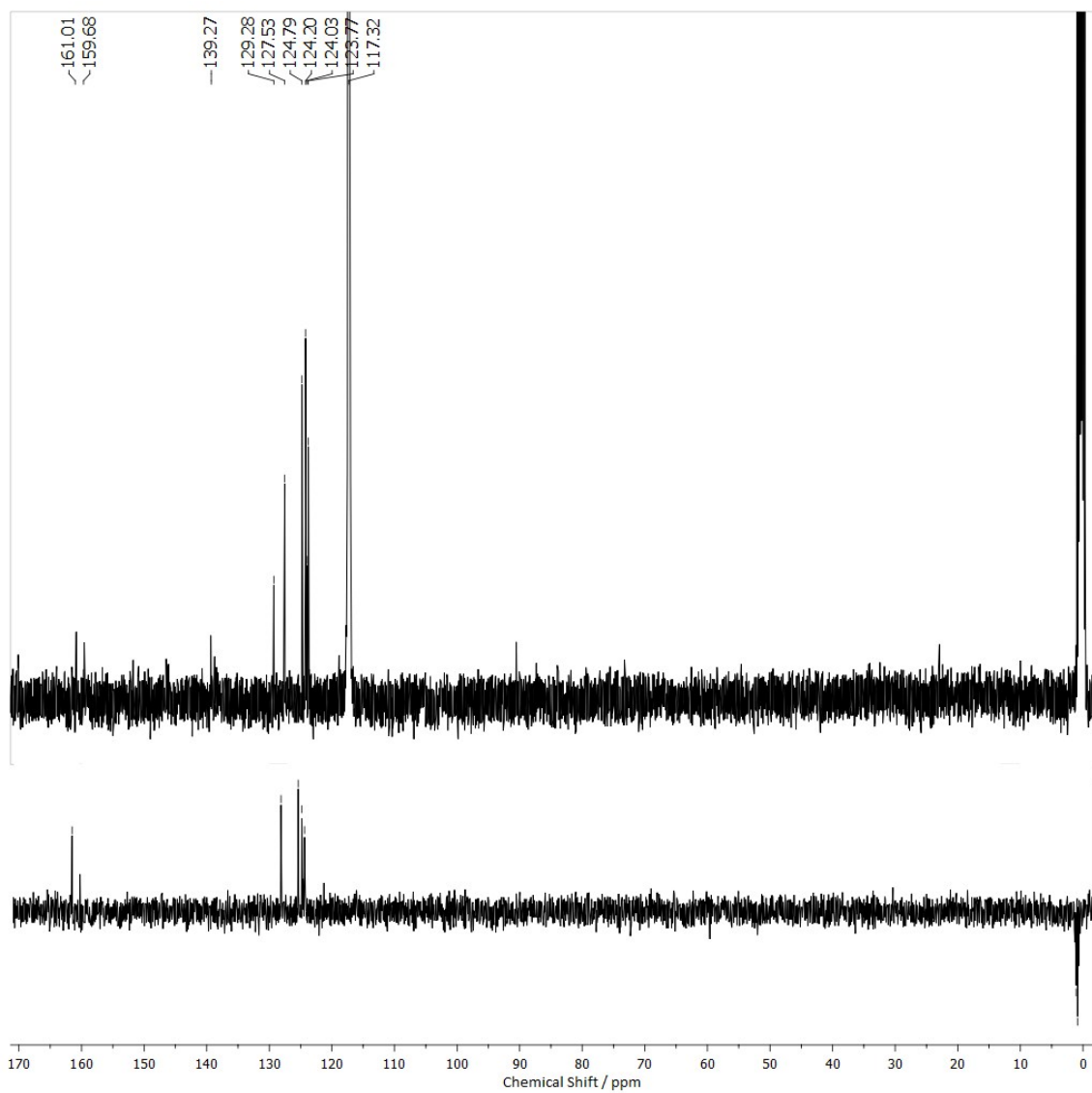
Figure S34 – ^{13}C NMR, at 100 MHz, (top) and DEPT-135 (bottom) spectra for **3e**.
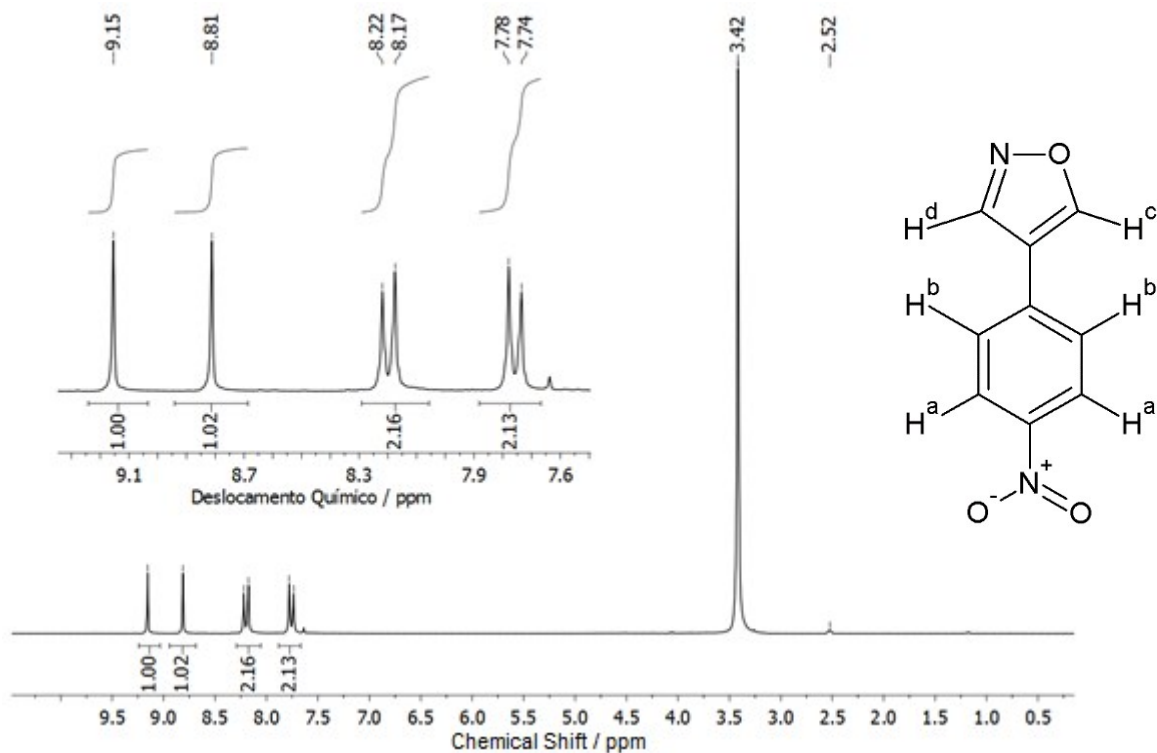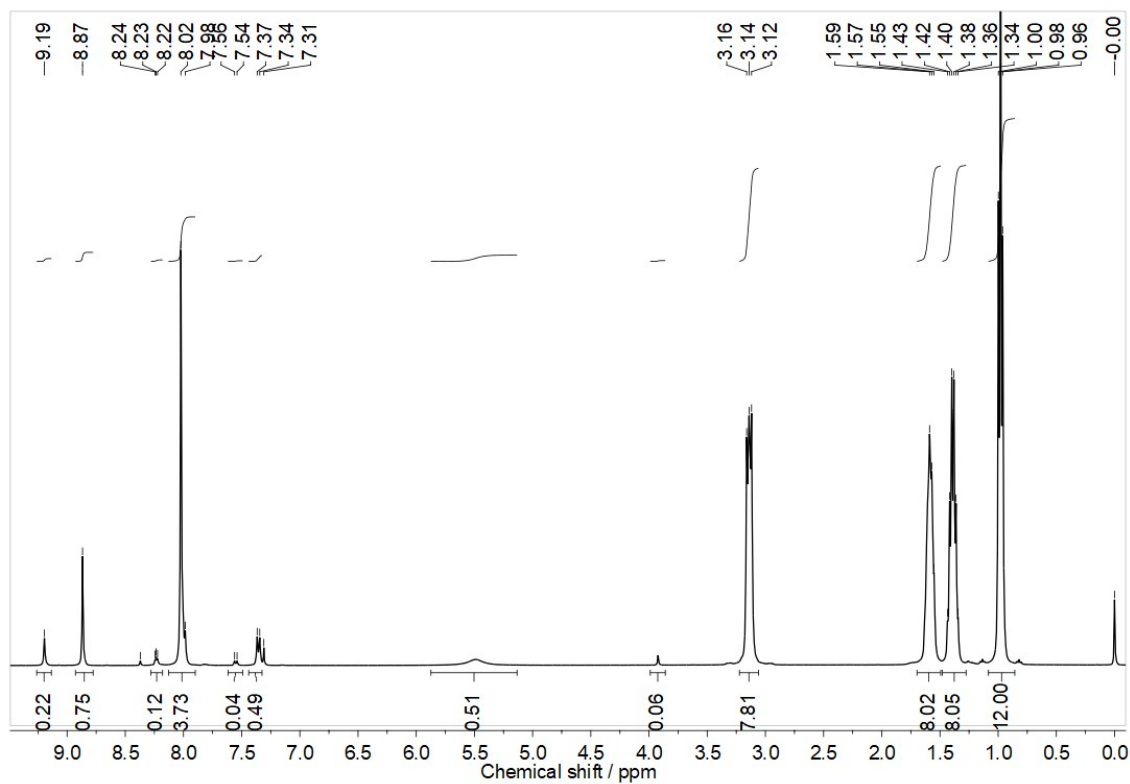
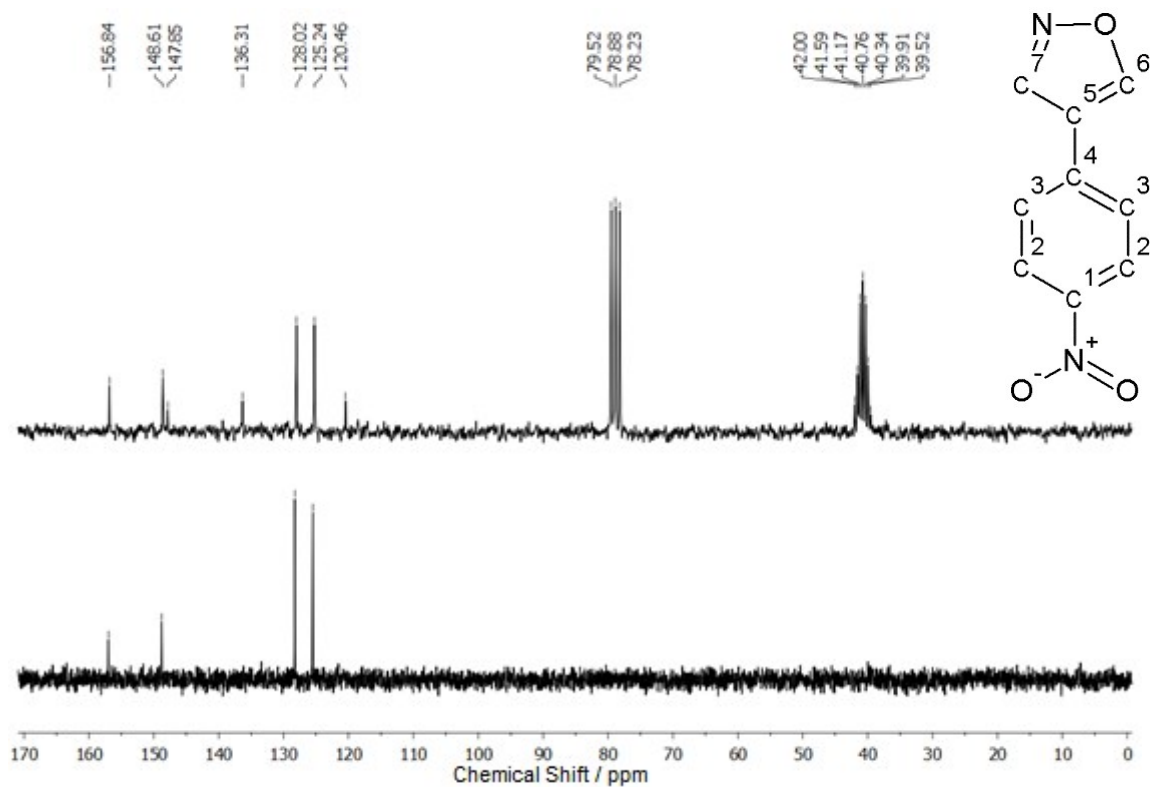**Figure S35** – ^{1}H NMR spectrum of **3f** in dmso-d$_6$ at 400 MHz.

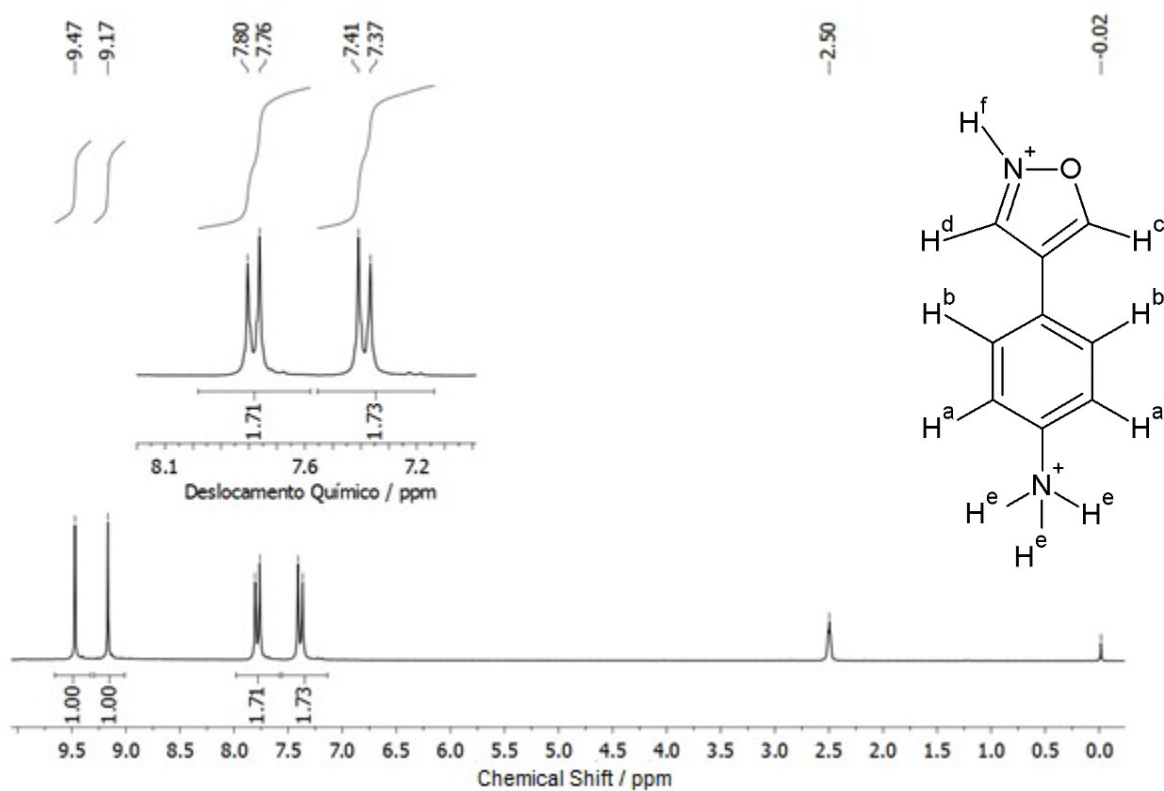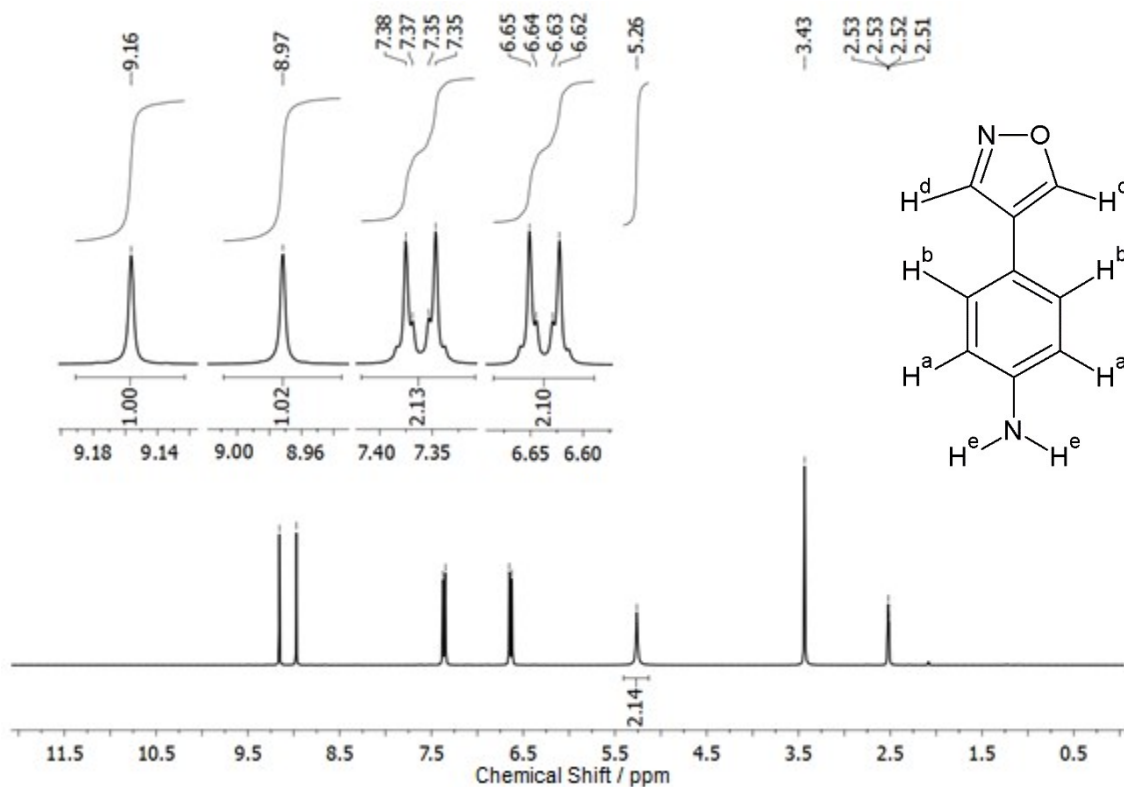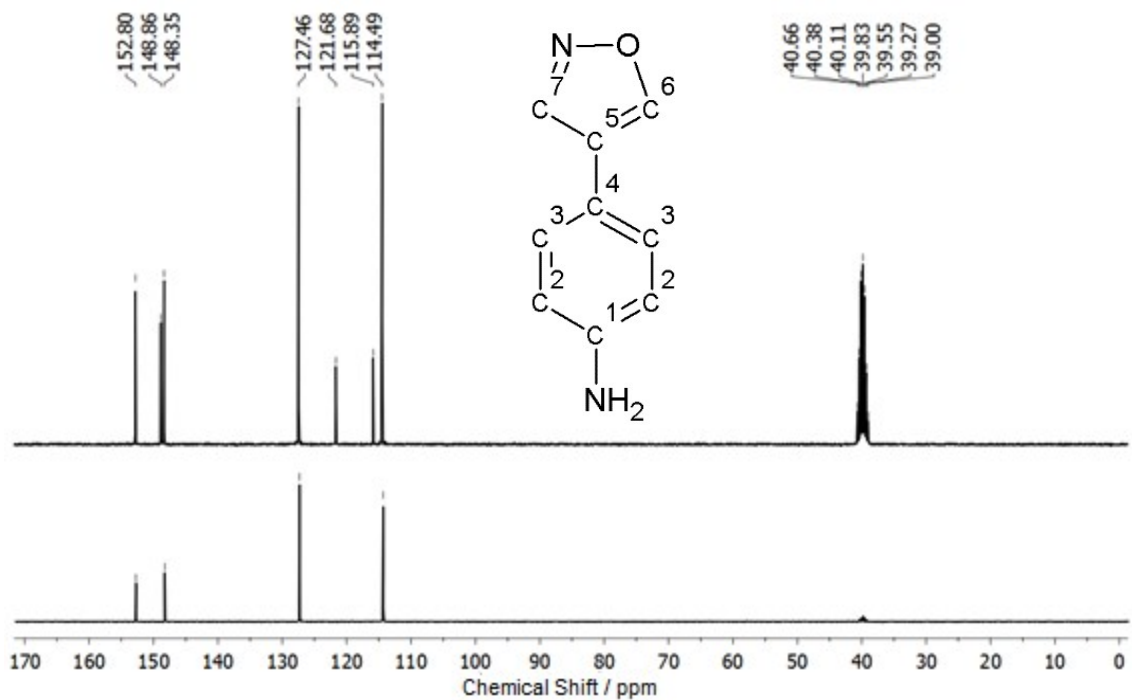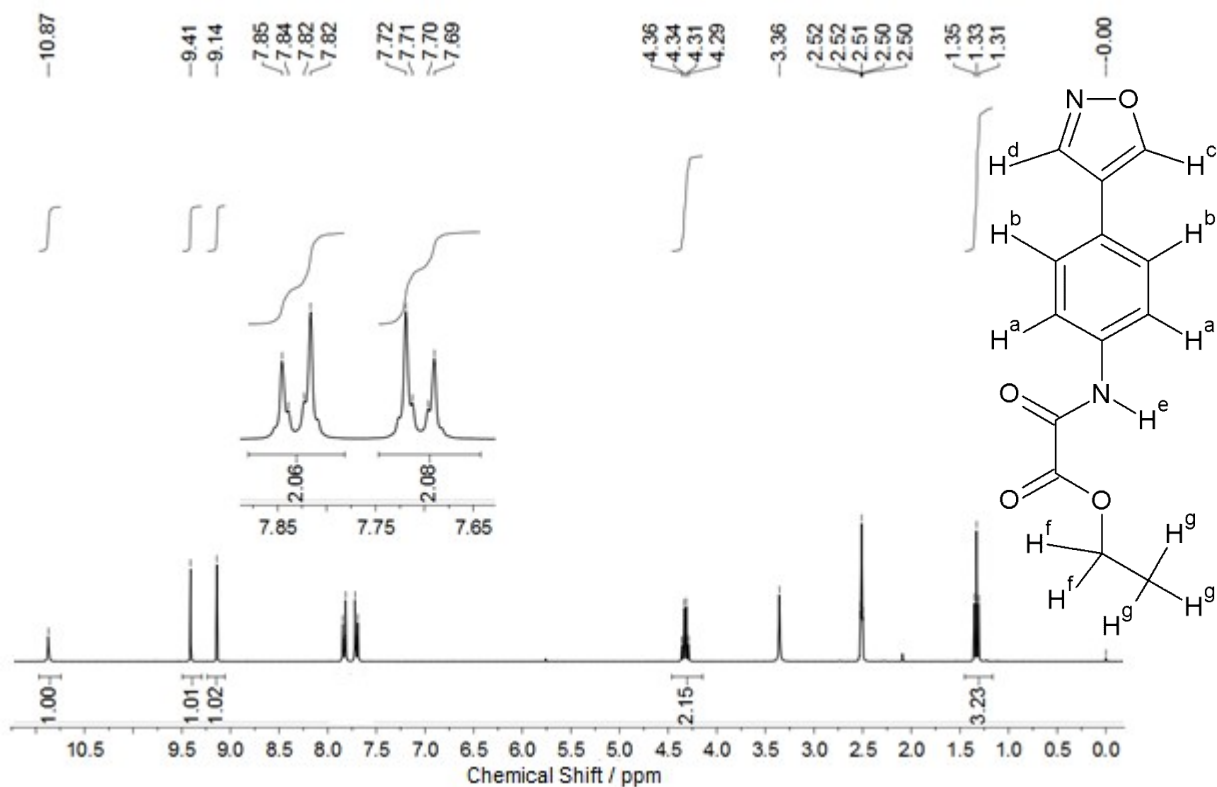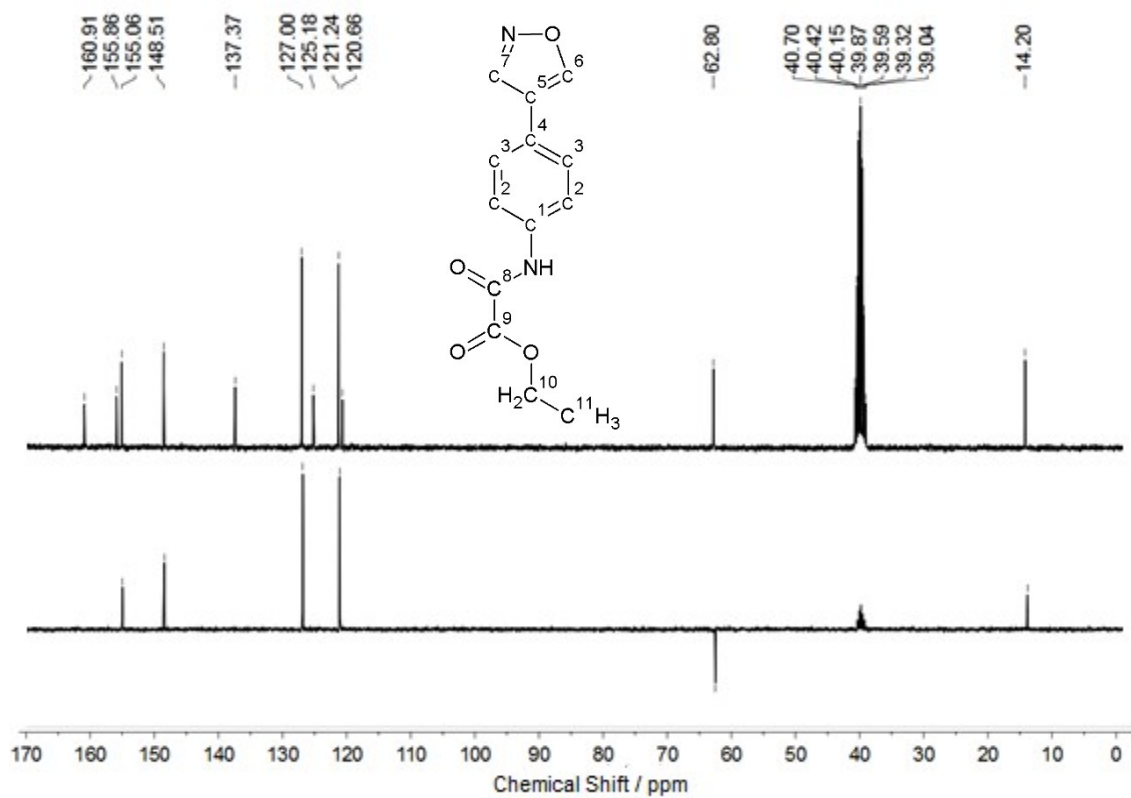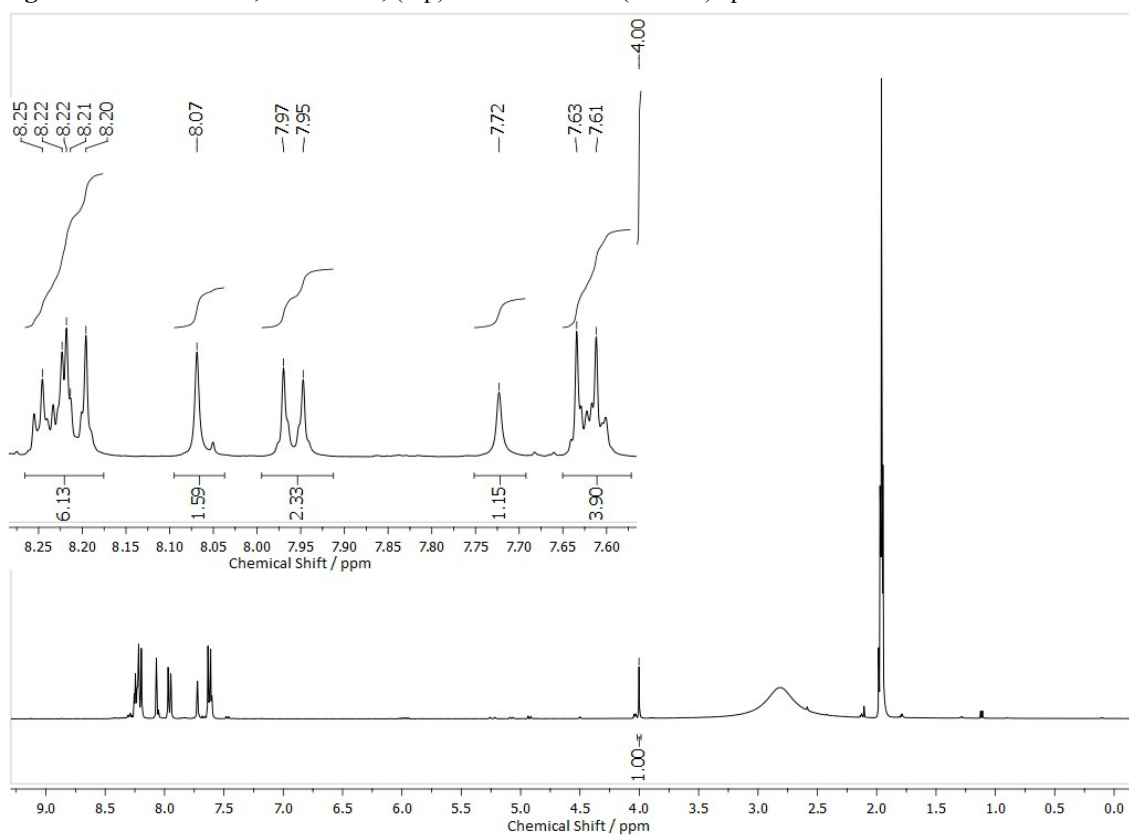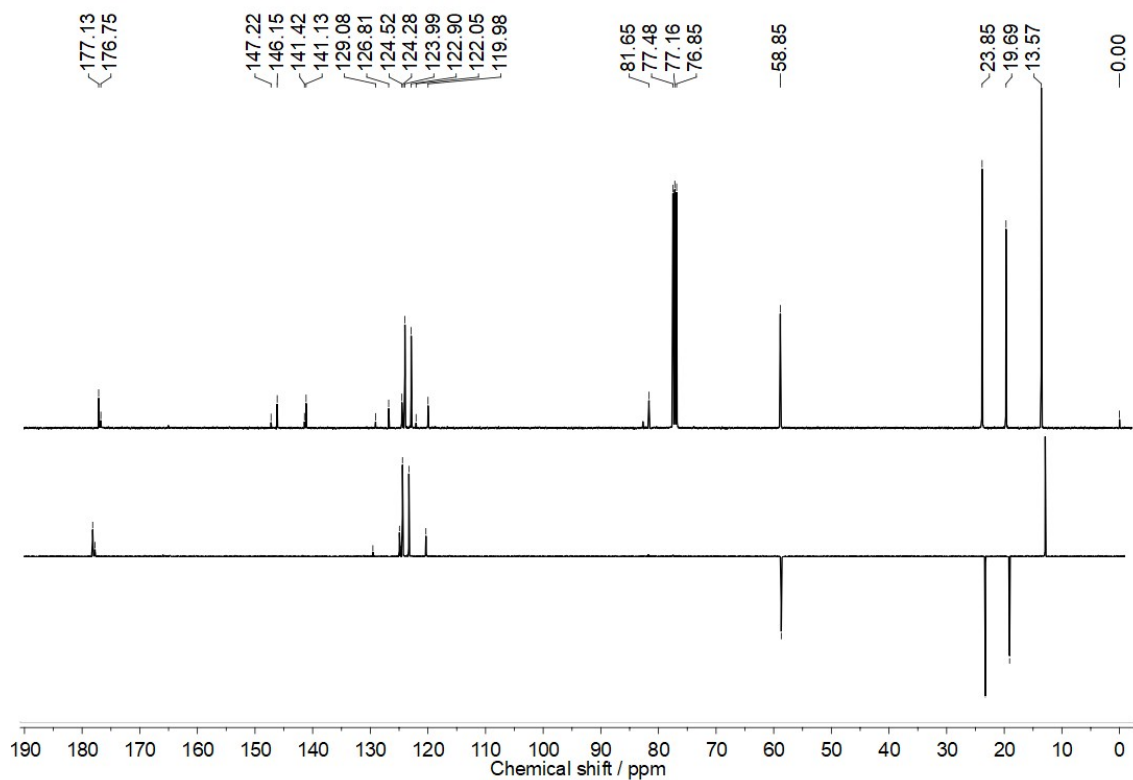**Figure S36** – ^{13}C NMR, at 100 MHz, (top) and DEPT-135 (bottom) spectra for **3f**.

Figure S37 – Comparison between the experimental X-ray powder diffraction pattern of **2b** (top, black line) and the pattern calculated from its crystal structure (bottom, red line).

Figure S38 – Comparison between the experimental X-ray powder diffraction pattern of **2e** at room temperature (top, black line) the patterns calculated using unit cell obtained from non-refined single crystal experiments at 300 K (middle, blue line) and fully refined crystal structure performed at 120 K (bottom, red line) emphasizing the shifts due lattice contraction upon cooling. The cell parameters at room temperature are: $a = 17.876$ Å, $b = 20.180$ Å, $c = 31.503$ Å, $\alpha = 90°$, $\beta = 104.577°$ and $\gamma = 90°$.

Figure S39 – Comparison between the experimental X-ray powder diffraction pattern of **3b** (top, black line) and the pattern calculated from its crystal structure (bottom, red line).

Figure S40 – Comparison between the experimental X-ray powder diffraction pattern of **3d** (top, black line) and the pattern calculated from its crystal structure (bottom, red line).
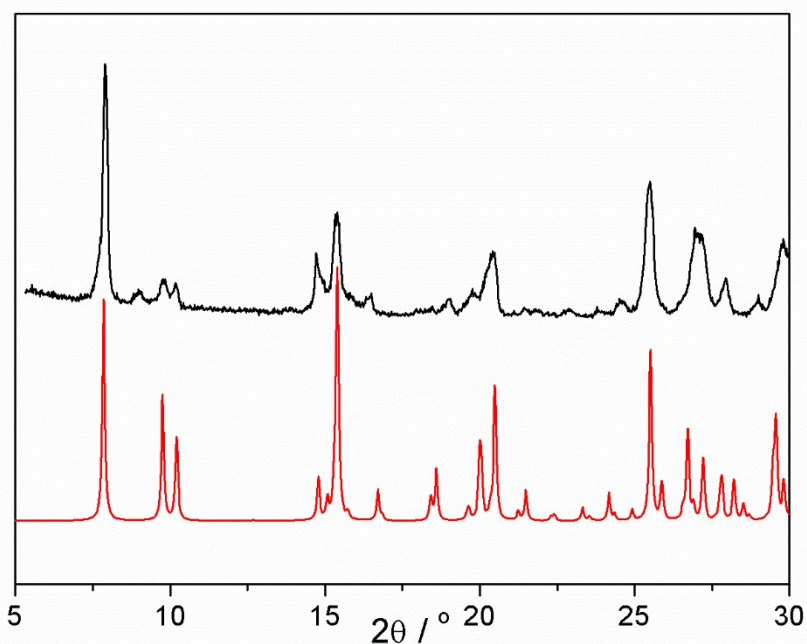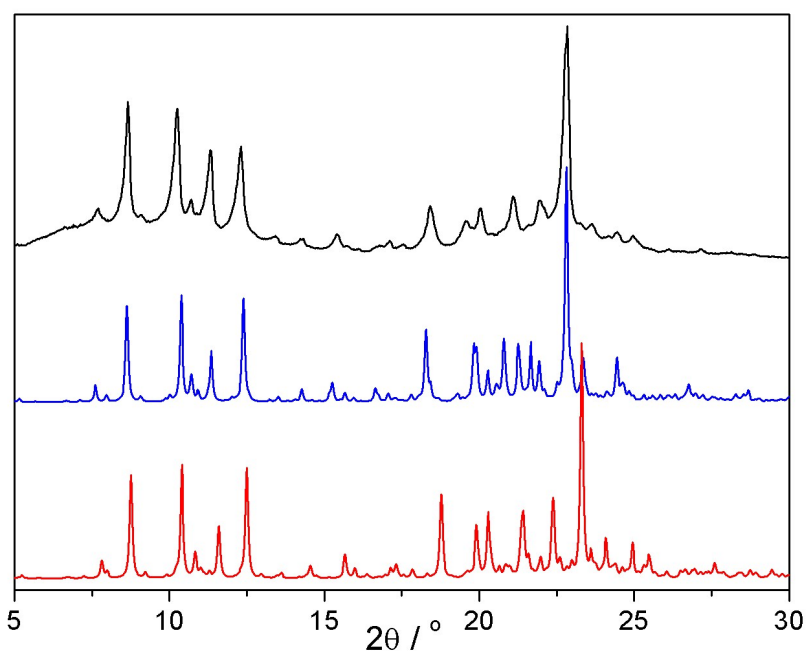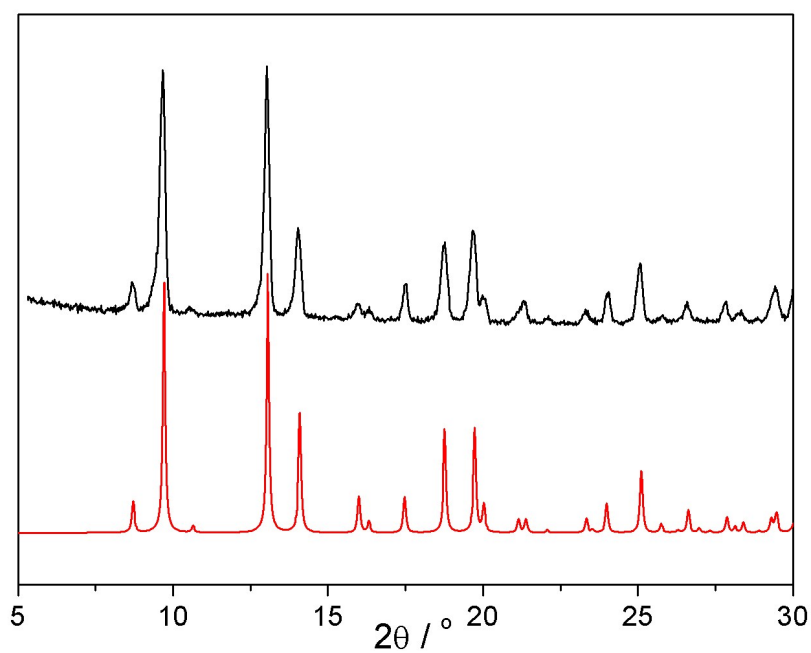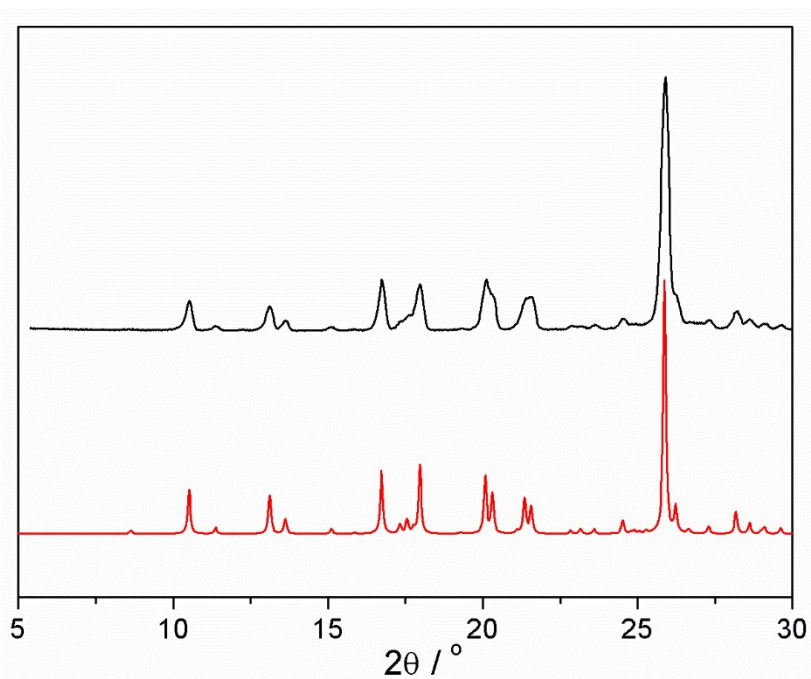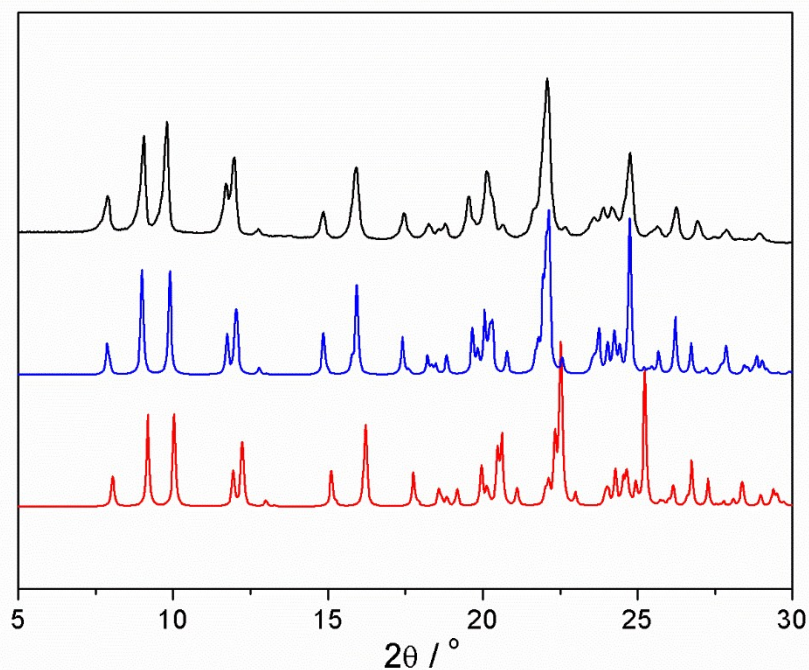
Figure S41 – Comparison between the experimental X-ray powder diffraction pattern of **3f** at room temperature (top, black line) and the patterns calculated using unit cell obtained from non-refined single crystal experiments at 300 K (middle, blue line) and fully refined crystal structure performed at 120 K (bottom, red line) emphasizing the shifts due lattice contraction upon cooling. The unit cell parameters at room temperature are: $a = 11.999$ Å, $b = 9.756$ Å, $c = 22.526$ Å, $\alpha = 90°$, $\beta = 99.231°$ and $\gamma = 90°$.
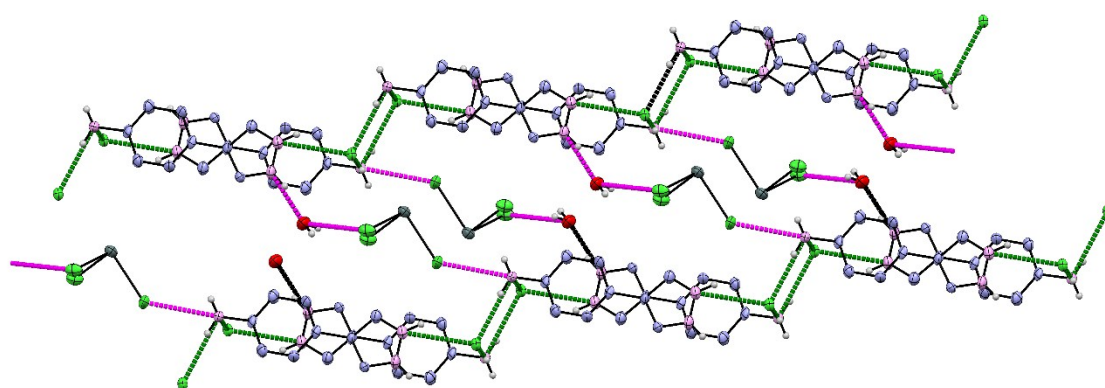
Figure S42 – View of a fragment of two supramolecular chains in **2b** featuring the hydrogen bonds connecting them via H_2O and $[SnCl_3]^-$ (pink lines). Green lines represent the hydrogen bonds between the organic cation and the chloride anions which build up the ladder-like supramolecular double chains.

Figure S43 – View of a fragment of two adjacent supramolecular chains in **2b** featuring the π-π stacking between them (red lines). Red spheres represent the geometric center of ring. Green lines stand for the

hydrogen bonds between the organic cation and chloride anions which build up the ladder-like supramolecular double chains.
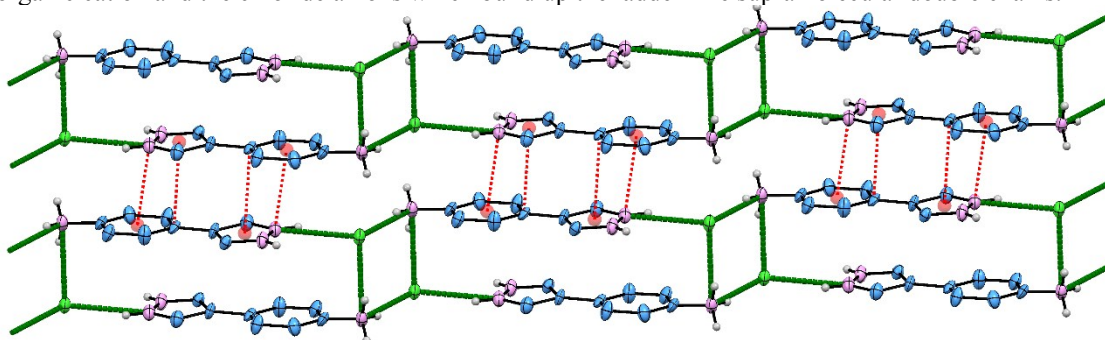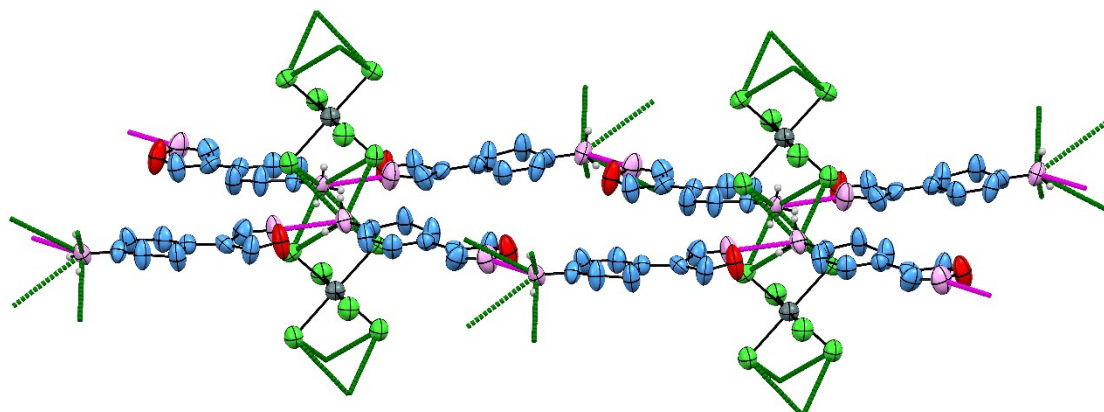

Figure S44 – View of a fragment of two adjacent supramolecular chains in **3b** featuring the hydrogen bonds between the organic cation and the coordinated chlorine atom in the $[SnCl_6]^{2-}$ unit connecting them. Pink lines stand for the hydrogen bonds between the organic cations, meanwhile green lines are for ammonium to $[SnCl_6]^{2-}$, which together build up the supramolecular chain.
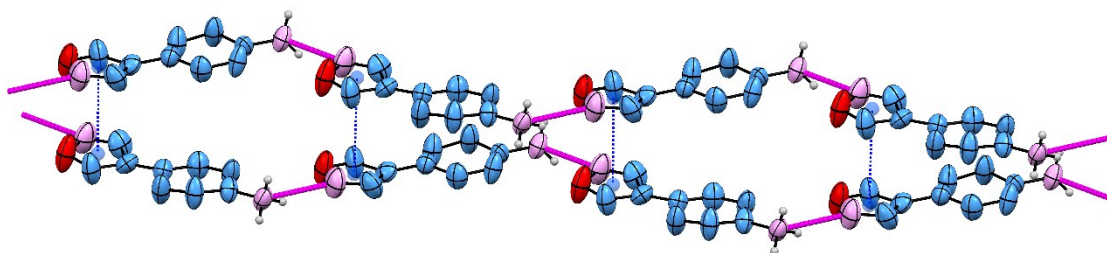
Figure S45 – View of a fragment of two adjacent supramolecular chains in **3b** featuring the π-π stacking between them (blue lines). Blue spheres represent the geometric center of the ring. Pink lines stand for the hydrogen bonds between the organic cations which build up the supramolecular chain.

Figure S46 – Crystallographic independent *n*-tetrabutylammonium cations of **2e** showcasing their different aliphatic chain conformation. C92 and C55 atoms are found disordered occupying more than one position and thus more than one conformation for its chain.

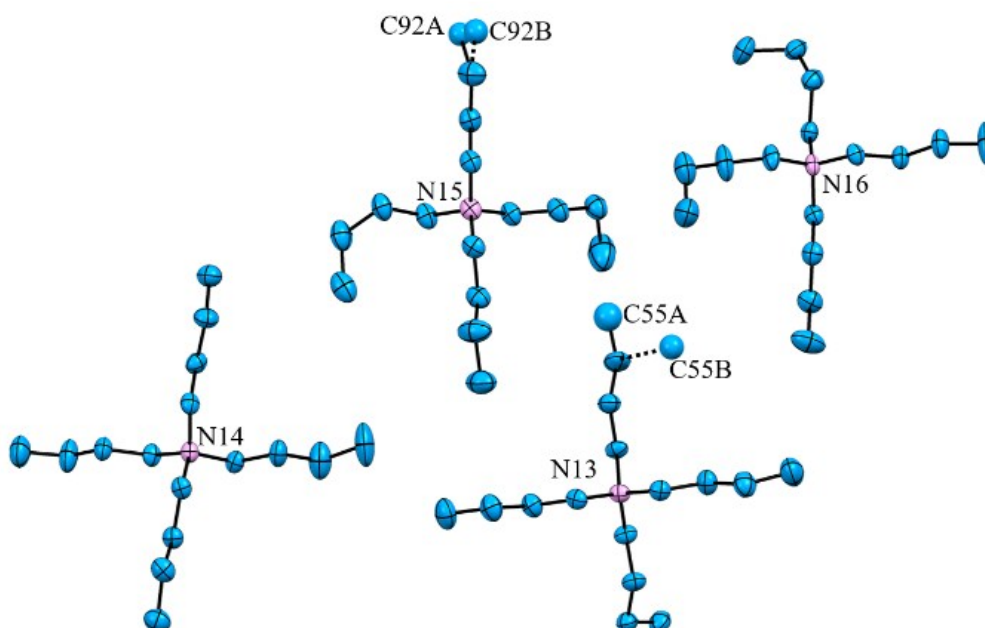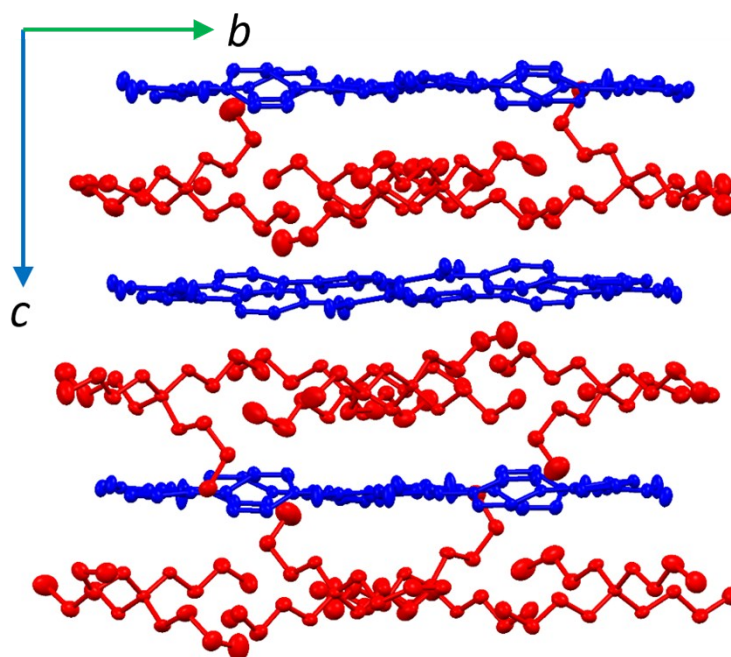**Figure S47** – Crystal packing of **2e** down the crystallographic *a* axis featuring the hydrophobic cationic (red) and hydrophilic anionic (blue) layers in an alternated stacking.

Upon heating, **2b** is stable between room temperature and 45 °C when the first weight loss was observed (Figure S48). In this fist event, 4.0% of initial mass is lost, which is equivalent to one water molecule (calc. 4.1%). The dehydrated material is thermally stable between 80 °C and 150 °C, when new weight losses events take place, probably due to organic and inorganic matter decomposition. A plateau is reached at about 550 °C with residue correspondent to 14.0% of initial mass.

Compound **2e** is thermally stable up to 70 °C, when, upon heating between 70 and 100 °C, a weight loss of 1.3% of initial mass is lost (Figure S49). This lost is related to evaporation of 0.5 water molecule, which corresponds to 1.6% of **2e** molecular weight. The product is thermally stable up to 220 °C. Above 220 °C, a great weight loss is observed, remaining at 300 °C of a residue correspondent to 39.1% of initial mass.

The thermogravimetric analysis for **3b** showed its thermostability upon to 160 °C. Between 160 and 600 °C, several events were observed, probably related to organic and inorganic moieties decomposition (Figure S50). The analysis residue, observed at 600 °C corresponds to 25.2% of initial mass and it can be associated to metallic tin, which corresponds to 28.9% of **3d** molecular weight.
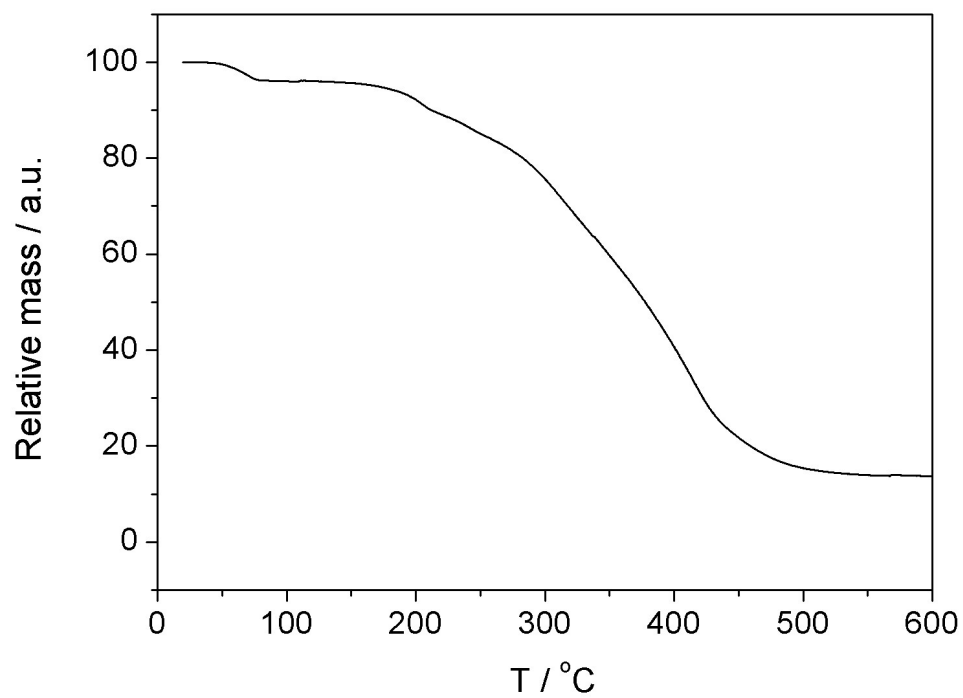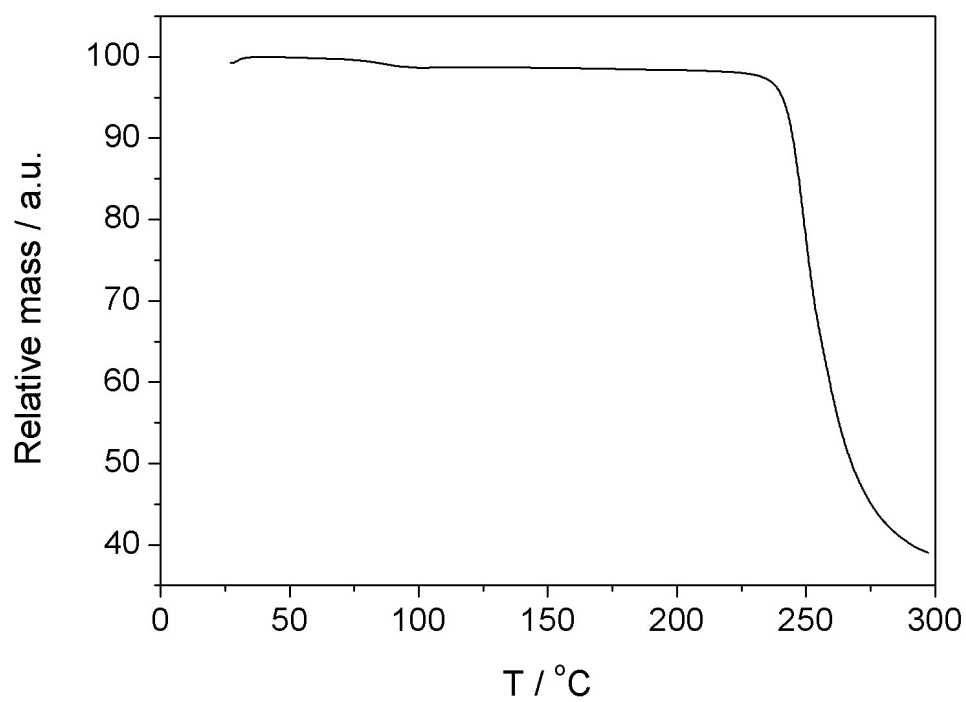
Figure S48 – TGA curve for **2b**.
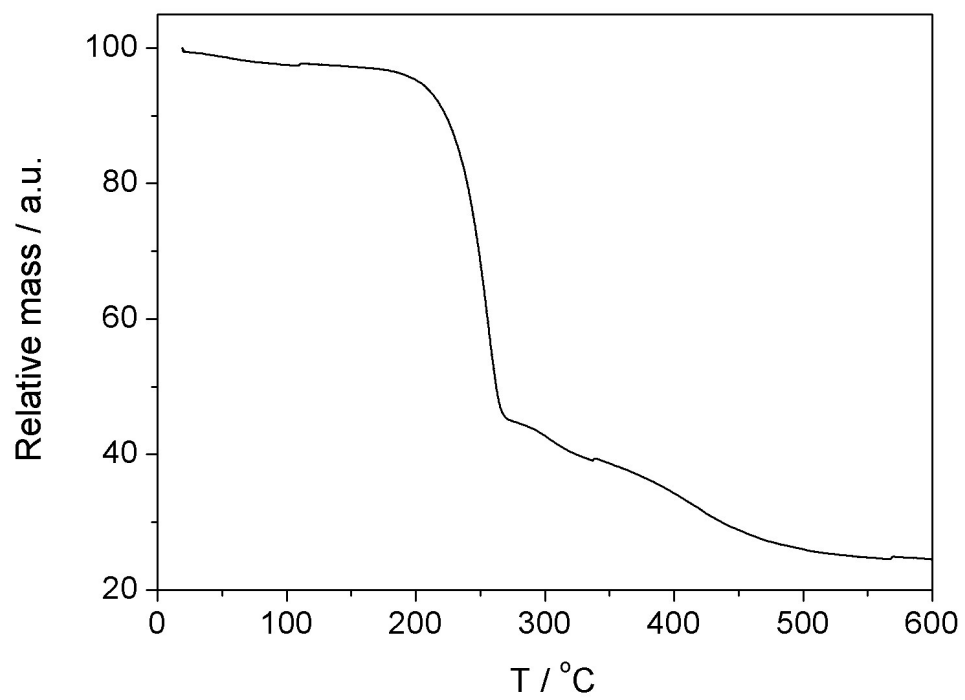

Figure S49 – TGA curve for **2e**.

Figure S50 – TGA curve for **3b**.